ORIGINAL RESEARCH ARTICLE

Transition to Sustainable Iron Production by EASyMelt: A Comprehensive Techno-Economic Study

FLORENT MAURET, MEHDI BANIASADI, JIHONG JI, PETER KINZEL, and HENRIK SAXÉN

Although the blast furnace process is the largest source of CO_2 emissions in the steel industry, it remains dominant due to its high productivity, cost-effectiveness, and flexibility in ore usage. Still, as CO_2-reduction policies expand, the steel industry and consequently the blast furnace must evolve toward significantly lower emissions. For this purpose, Paul Wurth S.A. has unveiled EASyMelt, a stepwise solution to cut blast furnace CO_2 emissions by integrating multiple cutting-edge carbon-reduction technologies, such as reducing gas injection, top-gas recycling, gas reforming, and plasma heating. This study introduces the EASyMelt concept and provides a comprehensive techno-economic assessment of multiple implementation pathways, each using a different combination of energy vectors such as coke oven gas, natural gas, pure hydrogen, ammonia, and hot briquetted iron. Leveraging a multi-fluid numerical model, the analysis reveals that EASyMelt scenarios significantly impact the furnace's thermal state, chemical behavior, and cohesive zone characteristics. Understanding these factors is critical to ensure successful and efficient implementation. EASyMelt deployment using natural gas and coke oven gas is found to reduce CO_2 emission of crude steel production by 47 pct while delivering operational expenditure savings at the current European carbon price of 72 €/t_{CO2}. Further integration of green energy vectors further enhances the environmental benefits: ammonia addition achieves a 63 pct reduction, hydrogen reaches 64 pct, and a combination of ammonia and hot briquetted iron push savings to 70 pct. While these advanced configurations require slightly higher carbon prices to maintain operational expenditure parity, such levels are likely to be reached shortly.

https://doi.org/10.1007/s11663-026-04022-2
© The Author(s) 2026

I. INTRODUCTION

STEEL is a foundational material for modern infrastructure and economic development. However, its production carries a steep environmental cost, contributing approximately 7 pct of global CO_2 emissions.[1] This makes the steel industry a major driver of climate change. All around the world new policies and mechanisms are being implemented to compel steep reduction in CO_2 emissions, putting the steel industry under ever-increasing pressure. Yet, decarbonizing steel is particularly challenging due to the industry's reliance on carbon-intensive processes.

The blast furnace–basic oxygen furnace (BF–BOF) route currently accounts for more than 70 pct of global crude steel production,[2] with the majority of the steel industry CO_2 emissions stemming from the BF process.[3] Nevertheless, rapidly phasing out this production route while meeting global steel demand is nearly impossible, given the blast furnace's current dominance, high productivity, thermodynamic efficiency, cost-effectiveness, and versatility in processing diverse iron ores and integrating different energy sources. Furthermore, even if some regions are better positioned to phase out the blast furnace process, steel remains a strategic resource due to its central role across all sectors of the economy. As a result, many countries are reluctant to depend entirely on foreign steel production, making the transition politically sensitive. As a result, reducing CO_2

FLORENT MAURET is with the Green Iron Making Team, Paul Wurth S.A., 32 Rue d'Alsace, 1122 Gare Luxembourg, Luxembourg and also with the Process and Systems Engineering, Åbo Akademi University, Henrikinkatu 2, 20500 Turku, Finland. Contact e-mail: florent.mauret@sms-group.com MEHDI BANIASADI, JIHONG JI, and PETER KINZEL are with the Green Iron Making Team, Paul Wurth S.A. HENRIK SAXÉN is with the Process and Systems Engineering, Åbo Akademi University.

Manuscript submitted October 24, 2025; accepted February 20, 2026.

Article published online March 18, 2026.

emissions from the blast furnace process is critical not only to meet global climate goals but also to ensure that the steel industry can satisfy growing demand for steel while remaining cost-competitive. Yet, traditional blast furnace operation is a mature technology and both energy utilization and greenhouse gas emissions are close to their theoretical minimum. Fundamental changes are therefore required to achieve a significant reduction of the process environmental impact. The past few years have seen a proliferation of innovative initiatives seeking to fundamentally enhance the blast furnace process, with the goal of achieving substantial reductions in CO_2 emissions. A comprehensive review of these efforts can be found in Reference 4.

Enhancing hydrogen use in the blast furnace is one of the key avenues for decarbonizing steel production.[5] A potential way to achieve this is by tuyere injection of hydrogen-containing media in the furnace, such as coke oven gas (COG),[6,7] natural gas (NG),[6,8,9] or waste plastics.[10] Injecting a hydrogen-containing medium free of carbon offers the greatest potential for CO_2 emissions reduction, with pure hydrogen[11,12] and cracked ammonia[13] recently gaining significant interest. These research efforts have already led to the industrial implementation of NG and, more recently, COG injection in industrial blast furnaces,[6] delivering substantial CO_2 savings. Unfortunately, the amount of hydrogen-rich medium that can be injected in the BF tuyere is limited by the heat shortage it causes in the shaft and throat of the furnace.[11,14] To go further in the decarbonization pathway, a secondary gas injection into the furnace shaft has been proposed as a promising solution. Tested over 50 years ago,[15] this technology has attracted renewed interest in response to the escalating urgency of the climate crisis.[16,17] Another thing to consider is that when large quantities of hydrogen-rich media are introduced into the blast furnace, the resulting top gas becomes increasingly valuable, prompting exploration into various strategies for its proper utilization or recovery. The most straightforward way is to recycle the top gas into the furnace's tuyere and/or shaft.[13,18] While simple, this approach faces practical limitations: recycling top gas with relatively high amount of CO_2 reduces the raceway flame temperature and impairs the reduction kinetics, restricting its applicability. The direct removal of CO_2 by carbon capture allows for a significant increase in the amount of top gas that can be recycled as demonstrated in the ULCOS project[19] where a 24 pct carbon saving was achieved. Further CO_2 reduction can be achieved by additional input of an external reductant, such as H_2 or NH_3. Another option for the removal of CO_2 from BFG is to use it in a dry gas reforming process.[20] The CH_4 in NG and/or COG reformed by the CO_2 present in the BFG, producing a syngas rich in H_2 and CO. This approach was first explored within the NKG process, where reducing gas was generated at approximately 1200 °C.[21] More recent developments have aimed to eliminate the need for catalysts by raising operating temperature to around 1450 °C through careful design of the dry-reforming stoves.[22] Thanks to the use of NG and COG, this approach addresses the issue of limited BFG availability, without requiring H_2/NH_3 input. A final option, proposed by JFE,[23] involves synthesizing methane using pure hydrogen and the CO_2 contained in the top gas *via* the Sabatier reaction.

In addition to enhancing hydrogen utilization in the furnace, increasing the temperature at which syngas is injected at the tuyere offers another lever for reducing emissions. Conventional hot stoves can typically reach temperatures around 1250 °C, while syngas dry reformers, due to their distinct mechanical characteristics, can achieve temperatures of up to 1450 °C. However, for higher carbon savings, syngas injection at the tuyere should occur at temperatures around 1700 °C to 2200 °C. This would significantly reduce the need for carbon combustion at the tuyere, while still ensuring that the resulting flame temperature remains below the critical threshold of 2250 °C to 2300 °C, which should not be exceeded to avoid issues such as refractory damage. To reach such high injection temperatures, heating by plasma torches have been proposed as a promising solution. The concept of using plasma torches to heat blast furnace tuyere gas dates back to the 1970s,[24] but has not been widely adopted at an industrial scale due to economic constraints. However, recent advancements in plasma torch technology, combined with stronger incentives to reduce CO_2 emissions, have renewed interest in this approach, making it increasingly attractive for industrial applications.

Charging hot briquetted iron (HBI) in the blast furnace is another option to reduce CO_2 emissions. Kobe Steel has recently conducted a large-scale HBI charging campaign,[25] achieving an 18 pct reduction in CO_2 emissions by charging 305 kg/t_{HM} while keeping production constant. As a carbon-free source of energy, biomass is also an interesting option, as reviewed in Reference 26; it could, for example, replace pulverized coal (PC).[27] However, regardless of technical and pre-treatment considerations, the scale of energy required by the blast furnace process makes biomass availability in most parts of the world a limiting factor, restricting its potential to only a partial solution.

Finally, because coke plays a critical role in supporting the burden and maintaining gas and liquid permeability within the blast furnace, it cannot be entirely replaced. As a result, some levels of CO_2 emissions remain unavoidable, regardless of the carbon avoidance measures implemented. To achieve net zero steel, Carbon Capture and Storage (CCS) must be deployed as a last step to eliminate residual, hard-to-abate emissions. A detailed discussion of the technical and economic aspects of CCS application to the BF can be found in References 28, 29. While CCS could theoretically be used as the sole decarbonization strategy, this would entail significant regulatory and social acceptance risks.[30] It appears more prudent to reserve CCS for addressing last-mile hard-to-abate emissions, when cost-effective direct carbon-saving options have been exhausted.

This paper provides a comprehensive techno-economic study of the Electrically Assisted Syngas sMelter (EASyMelt) concept, a resource flexible and cost-effective approach to decarbonize existing blast furnace

worldwide. The approach strategically integrates multiple CO_2 reduction technologies, in particular multi-level gas injection, top gas recycling, plasma heating for direct electrification, and gas reforming, with the aim to drastically reduce the BF environmental impact. The EASyMelt concept will first be introduced, in particular detailing how various green energy vectors can be integrated into it. Following this, different possible configurations of EASyMelt are investigated. The assessment focuses on how these scenarios influence overall furnace performance and the internal process state compared to conventional operation. For an in-depth understanding, the projected impact of the different implementations on energy usage, CO_2 emissions, and operational expenditures (OPEX) for crude steel production at the integrated steel plant is also reviewed. The processes data that the analysis is based on were obtained using a two-dimensional blast furnace model, called BFinner, presented in References 13, 14.

II. EASYMELT TECHNOLOGY

A. *Introduction to the Technology*

EASyMelt, developed by Paul Wurth S.A., is a breakthrough technology designed to reduce CO_2 emissions in blast furnace ironmaking. It can be implemented in a stepwise fashion, reducing risk and ensuring cost-efficiency across diverse economic conditions. An overview of the full implementation of the technology is shown in Figure 1. As part of the process, a reducing gas is generated *via* dry reforming of methane and heavier hydrocarbons from NG and/or COG, using recycled blast furnace top gas as the source of CO_2. Hydrogen-rich gases devoid of carbon, such as pure hydrogen or cracked ammonia, can also be added to the feed mixture for greater CO_2 savings. Syngas dry reformers operate in a cyclical manner, similar to conventional hot stoves. Each cycle consists of a heating phase, during which BFG is combusted to raise the reformer's temperature, followed by a reforming phase, where the feed gas is heated and converted into syngas. Owing to their specialized design and mechanical properties, these reformers can achieve gas temperatures of approximately 1450 °C, which is necessary to ensure efficient reforming operation without the use of a catalyst. The syngas obtained is then injected into the shaft and the bosh of the furnace. The gas injected at the shaft level is slightly cooled to around 1000 °C by recycling BFG, as the gas from the syngas reformers would otherwise be too hot. By contrast, the bosh gas is heated using plasma torches to 1700 °C to 2200 °C. This partial electrification of the ironmaking process drastically decreases the amount of coke that needs to be combusted in the raceway as most of the energy demand is satisfied by the heated syngas, while the hot blast is eliminated. Still, some oxygen injection is kept to help maintain a proper raceway shape. EASyMelt retains the flexibility of conventional blast furnaces in terms of ore usage, allowing the use of sinter, lump ore, or pellets, as well as the option to charge HBI.

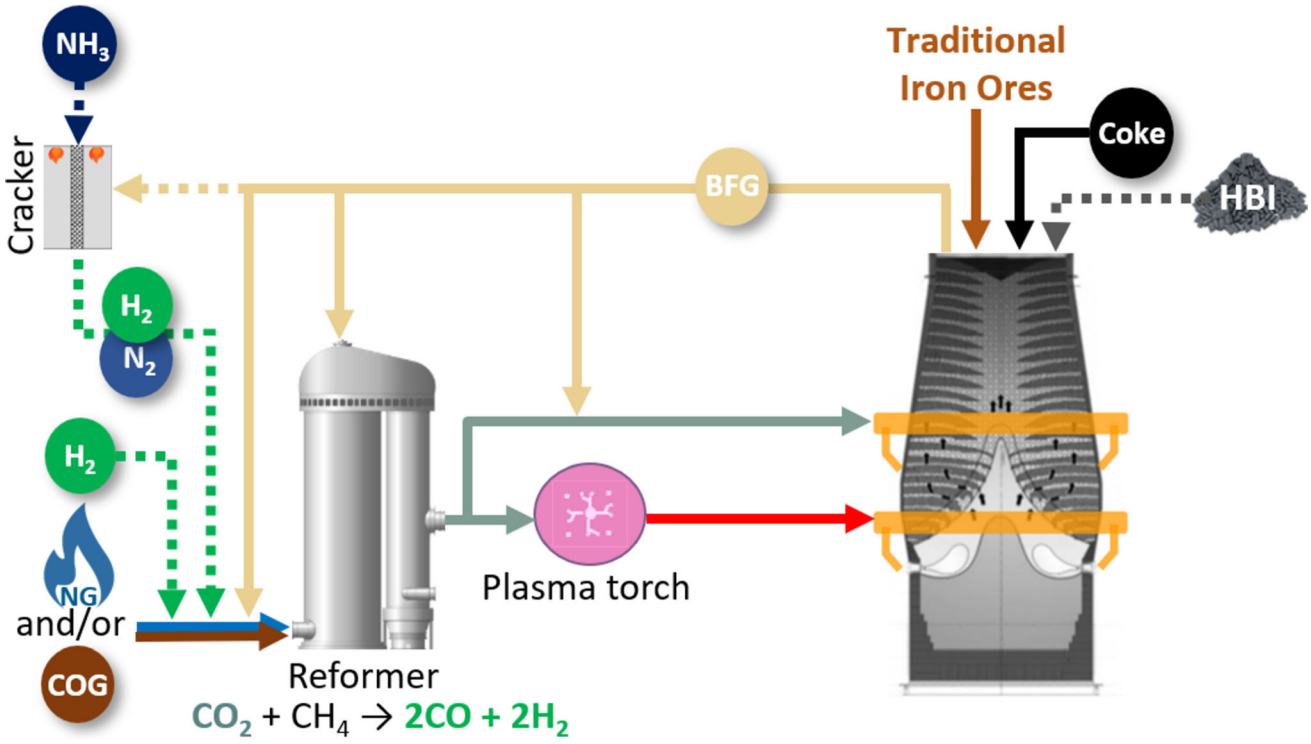


Fig. 1—Overview of EASyMelt technology with dry reforming and plasma torch. Dotted lines indicate optional additions.

B. H_2 Integration

Pure hydrogen can be seamlessly integrated into the EASyMelt process by introducing it into the syngas dry reformers, where it is heated together with the rest of the syngas. This strategy is particularly applicable to steel plants situated in regions with abundant renewable electricity resources and, as a result, cheap green hydrogen.

C. Ammonia Integration

The advantages of using ammonia as a hydrogen carrier have been thoroughly discussed in Reference 13, which focuses on its direct integration into blast furnace ironmaking. For completeness, a brief summary is provided below.

The price of green hydrogen will fluctuate across the world due to an uneven access to renewable energy. Nevertheless, it will not be possible to produce steel only where hydrogen price is low due to workforce availability, easy access to major transport routes, existing infrastructure, political decisions, etc. Thus, hydrogen will have to be transported to the required locations. Transforming green hydrogen to ammonia for long-distance transport is predicted to be more cost-effective than direct transport of liquid hydrogen in most scenarios.[31] This is true despite the additional conversion steps required to synthesize NH_3 and decompose it into H_2 and N_2 at the steel plant. Furthermore, using ammonia as hydrogen carrier is ideally adapted to blast furnace ironmaking. Indeed, hydrogen purity is not an issue for the BF process since the traditional process operates with a large share of nitrogen in the gas phase. Therefore, the gas obtained after ammonia cracking can be injected directly in the furnace, as done in Reference 13, or supplied to syngas dry reformers, as shown in Figure 1, in both cases without a need for cooling or separation. The heat required for cracking can also be obtained by burning BFG.

D. HBI Integration

The other main credible path for the decarbonization of steelmaking is through the direct reduction process using green hydrogen. Apart from its high investments costs, the two main barriers to the adoption of this technology are the high cost of green hydrogen[32] and the limited availability of high-grade iron ore pellets.[33]

Ammonia can similarly be used as a hydrogen carrier to help reduce cost for the direct reduction route. However, unlike blast furnace ironmaking, the direct reduction process requires high-purity hydrogen. The additional steps needed to purify hydrogen reduce supply chain efficiency and erode the cost advantage of using ammonia as a transport medium. A better approach is to carry out direct reduction using hydrogen in regions with abundant low-cost renewable energy and transport HBI instead. Selecting a location for a new greenfield DRI plant is indeed often easier, as it must be built from the ground up anyway.

HBI obtained from the direct reduction process can be used in different steelmaking processes, *e.g.*, in the electric arc furnace (EAF), in open bath furnace (OBF) or charged into BFs. In the case of EAFs, high-grade HBI is strongly preferred, as operating with lower-grade material poses significant challenges to process stability and efficiency.[34] To produce high-grade HBI, pellets of high quality have to be used in the DR process, but their availability is limited. On the other hand, BFs and OBF can operate efficiently with either low- or high-grade HBI, offering greater flexibility in the quality of pellets required by the DRI process. Even though OBF offers this flexibility, it requires bigger investment than BF since it must be built from scratch. When it comes to conventional BFs, the amount of HBI that can be fed into the furnace while maintaining a stable and efficient process is limited, and consequently, the potential CO_2 savings are constrained. The operation of EASyMelt is naturally similar to that of the conventional BF when it comes to flexibility in ferrous burden usage and can thus accept similar amount of HBI. Yet, EASyMelt can reach far greater emission savings due its other CO_2 saving technologies and is therefore a very promising option.

III. NUMERICAL MODEL

A. Description

The BFinner model was employed to evaluate the impact of different EASyMelt implementations on the internal state and overall performance of the blast furnace. Although the model has been described in detail elsewhere,[13,14] a brief overview is provided here for completeness.

BFinner is a multi-fluid 2D axisymmetric steady-state model, predicting the internal BF state from the stockline down to the liquid slag surface. Using a 2D axisymmetric domain is a widely adopted approach for blast furnace modeling, offering strong computational efficiency while still capturing the essential process behavior with good accuracy. Previous works have similarly employed a steady-state formulation,[35,36] with some studies attempting to extend the approach to transient simulations.[37]

Gas and solid phases, composed of multiple components, are treated as continuous fluids predicting their flow, heat and mass transfer, and chemical reactions. To reduce the computational effort, the flow of the liquid phase is not explicitly resolved. However, its influence on the thermal and chemical states of the other phases, as well as on furnace permeability, is accounted for as detailed in Reference 14. The governing equations of the model are given in Table I; for the detailed nomenclature, the reader is referred to Reference 13. The model calculates the key chemical reaction rates, including the indirect reduction of iron oxides by CO and by H_2, the direct reduction of FeO in the liquid phase by solid carbon, the burden moisture vaporization, the Boudouard, the water–gas and the water–gas shift reactions, as well as the melting processes involving Fe, FeO, and gangue components.

Table I. Governing Equations of BFinner Model for Solid and Gas Phases

Phase	Description	Equations
Solid	continuity	$\nabla \cdot (\rho_s u_s) = 0$
	momentum	$-K_b \nabla \phi = u_s,$ where $K_b(r_{ND}) = \frac{V_{s,top}(r_{ND})}{\max(V_{s,top})}$
	temperature	$\nabla \cdot (\rho_s u_s C_{p_s} T_s) = \nabla \cdot ((1-\epsilon)\lambda_{eb,s} \nabla T_s) + S_{s,H}$
		$S_{s,H} = hA_{g-s}(T_g - T_s) + \alpha(\kappa Q_{l,DZ} + \sum_{k=1}^{n_{react}} R_k \Delta H_k)$
	chemical species	$\nabla \cdot (\rho_s u_s w_i) = S_{w,i}$
		$S_{w,i} = \sum_{k=1}^{n_{react}} M_i R_k,$ where i = $Fe_2O_3, Fe_3O_4,$ FeO, Fe and Gangue
Gas	continuity	$\nabla \cdot (\rho_g u_g) = S_{s-g},$ where $S_{s-g} = -\sum_{k=1}^{n_{react}} \beta_k R_k$
	momentum	$-K_g \nabla p = u_g,$ where $K_g = \frac{1}{\mu_g + b\rho_g \lvert u_g \rvert}$
		$a = \frac{E_1(1-\epsilon)^2}{\Phi^2 d_p^2 \epsilon^3}$ and $b = \frac{E_2(1-\epsilon)}{\Phi d_p \epsilon^3}$
	temperature	$\nabla \cdot (\rho_g u_g C_{p_g} T_g) = \nabla \cdot (\epsilon \lambda_{eb,g} \nabla T_g) + S_{g,H}$
		$S_{g,H} = hA_{g-s}(T_s - T_g) + (1-\alpha)(\kappa Q_{l,DZ} + \sum_{k=1}^{n_{react}} R_k \Delta H_k)$
	chemical species	$\nabla \cdot (\rho_g u_g w_i) = \nabla \cdot (\rho_g \epsilon D_{eb,i} \nabla w_i) + S_{y,i}$
		$S_{y,i} = \sum_{k=1}^{n_{react}} M_i R_k,$ where i = CO, CO_2, H_2, H_2O and N_2
	ideal gas equation	$\rho_g = \frac{P \sum_i y_i M_i}{R(T_g + 273.15)}$

A flowchart of the model is presented in Figure 2. The burden distribution is first estimated by a charging model that has been extensively validated for industrial applications as part of the BFxpert® system.[38] Raceway conditions are then determined through an overall heat and mass balance, based on the assumption that the gas exiting the raceway consists solely of CO, H_2, and N_2. The model equations are initially solved without updating the location of the cohesive zone (CZ) until a preliminary convergence is achieved. Subsequently, the same equations are solved with iterative updates to the CZ location until a stricter convergence is reached. At this point, two situations may arise. If the objective is to predict a reference case with known operating conditions, the model results are compared with existing plant measurements to validate the predictions. Alternatively, if the analysis concerns a new process, such as the EASyMelt implementation scenarios examined in this study, the predicted coke rate and top gas composition are compared with the initial assumptions used to determine the burden distribution and the reducing gas composition. If the predicted coke rate deviates from the target, the burden distribution is updated accordingly by changing the ore-layer thickness. Similarly, if the top gas composition does not align, the reducing gas composition from the dry reforming process is adjusted based on the newly predicted BFG composition. The full loop is then repeated until both parameters are matched to sufficient accuracy. Care is also taken to ensure that the thermal conditions of the process remain acceptable, specifically, maintaining a suitable top-gas temperature, retaining an adequate heat input to achieve a reasonable hot-metal temperature, and preserving an appropriate cohesive-zone shape to support proper gas flow. If these conditions are not met, operating parameters such as the oxygen injection rate, syngas composition, tuyere syngas flow, or shaft-injected syngas flow are adjusted accordingly. Due to interactions between the manipulated variables, it is difficult to provide a comprehensive description of how each variable is adjusted. Broadly speaking, increasing the oxygen injection rate raises both the flame temperature and the heat input to the lower part of the furnace that is needed to achieve the desired production rate and proper hot metal temperature. Increasing the tuyere gas flow rate also increases the heat input to the lower part of the furnace, but it typically results in a lower flame temperature. Increasing shaft-injected syngas, which introduces thermal energy higher in the furnace, tends to raise the top-gas temperature. Although an infinite number of parameter combinations could theoretically be used to address the process thermal constraints, the adjustments are selected in an attempt to minimize CO_2 emissions and reduce the overall operating cost of the process.

B. *Validation*

Model validation is a critical step in confirming the accuracy and predictive capability of numerical simulations. In Mauret *et al.*,[14] a thorough validation of BFinner was conducted using data of a commercial BF under conventional operation. The model predictions were compared to top gas measurements, in-burden probe measurements, and pressure measurements at the

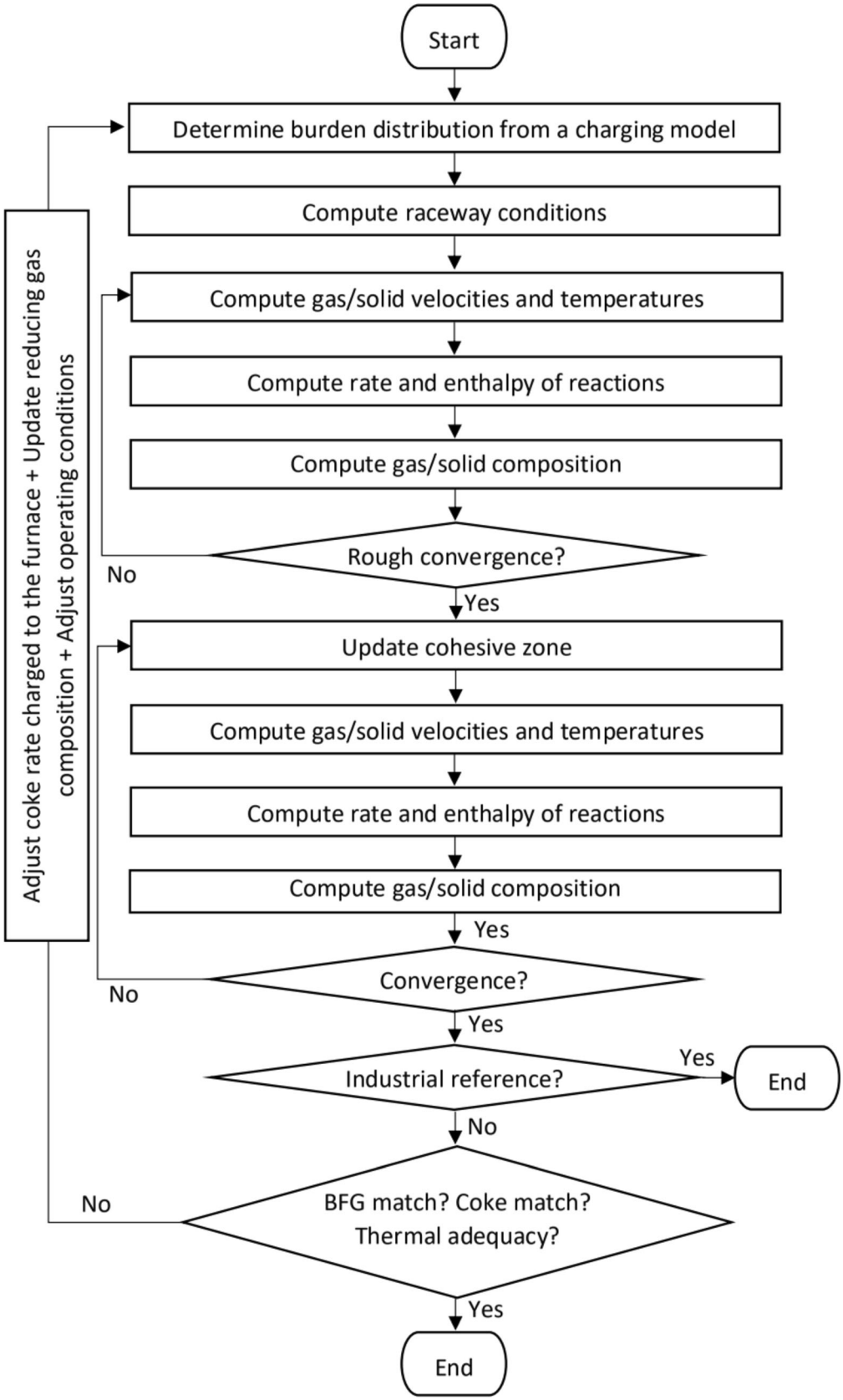


Fig. 2—Overall flowchart of BFinner model.

wall. The comparison was made for two different furnace states, illustrating the generic features of the model.

However, the EASyMelt processes are operating under significantly altered states, particularly due to the much higher H_2 content in the gas. Validation of BFinner for a BF process with a high hydrogen load is therefore desirable to give confidence in the model's predictive capability. This task is made difficult by the scarcity of data available for hydrogen-rich blast furnace operation. Fortunately, as part of the COURSE50 project, Nippon Steel has recently published a comprehensive set of data for a test on their 12 m^3 experimental BF operating with hydrogen-rich gas.[39] A validation of BFinner will be presented using data from Case C of Nippon Steel's fifth campaign. For this case, the total H_2 input was of 276 Nm^3/t_{HM}, with the injection of 170 Nm^3/t_{HM} of pure H_2 and 119 Nm^3/t_{HM} of COG. The details of the operating conditions are reported in Reference 39 while more information on the experimental BF characteristics are presented in References 12, 40.

The internal state of the experimental BF predicted by BFinner is shown in Figure 3. It can be seen that the gas coming from the tuyere is composed of approximately 18 pct of H_2. This high amount of hydrogen has a significant impact on the reduction processes in the furnace. Table II shows that the predicted distribution of the iron oxide reduction between the different reducing agents closely aligns with the observed operational data.

The experimental BF is also equipped with horizontal sampling probes located at three different levels. For a more thorough validation, Figure 4(a) compares the measured and predicted horizontal distributions of CO and H_2. The probe measurements, particularly at the lower level, exhibit asymmetry when comparing negative and positive distances from the center. This effect arises from the probe's position: at negative distances, it is located above a tuyere, whereas at positive distances, it lies between tuyeres. As the current model is two-dimensional and axisymmetric, such asymmetry cannot be captured. Nevertheless, the results obtained by BFinner fall between these two extremes, and the main trends are accurately reproduced, which can be considered satisfactory. Finally, Figure 4(b) presents the predicted vertical profiles of CO and H_2 concentrations, compared with measurements from a vertical probe. The predicted concentrations are color-coded according to their normalized radial positions. The vertical probes are introduced with the burden at the BF top and follow the burden as it descends. However, they do not necessarily move vertically and their radial position lower down in the furnace is therefore unknown. The fact that the measured values largely fall within the predicted ranges indicates a strong agreement between the model predictions and the experimental observations. Overall, the results of BFinner under high hydrogen load conditions demonstrate good agreement with the experimental findings and validate the model's generic capabilities.

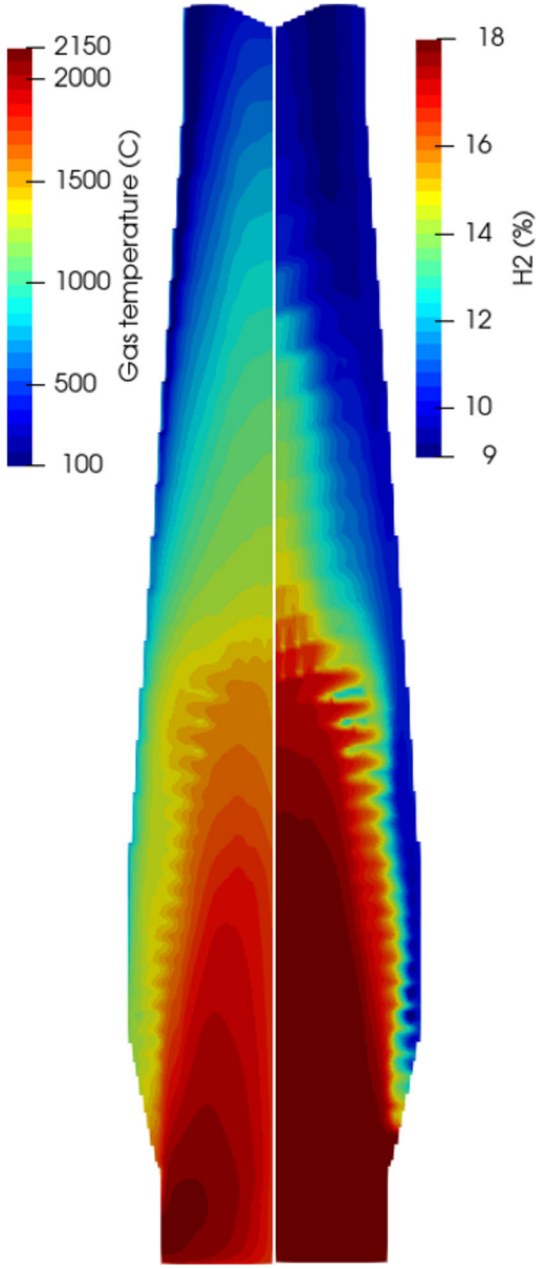


Fig. 3—Predicted thermal and hydrogen distribution of Nippon Steel experimental BF.

Table II. Comparison Between Predicted and Operational Ratios of Iron Oxides Reduction in Nippon Steel Experimental BF

	Predicted Data	Operation Data (Sourced from Ref. [39])
CO Indirect Reduction (Pct)	62.7	60.7
H_2 Indirect Reduction (Pct)	24.0	24.0
Carbon Direct Reduction (Pct)	13.3	15.3

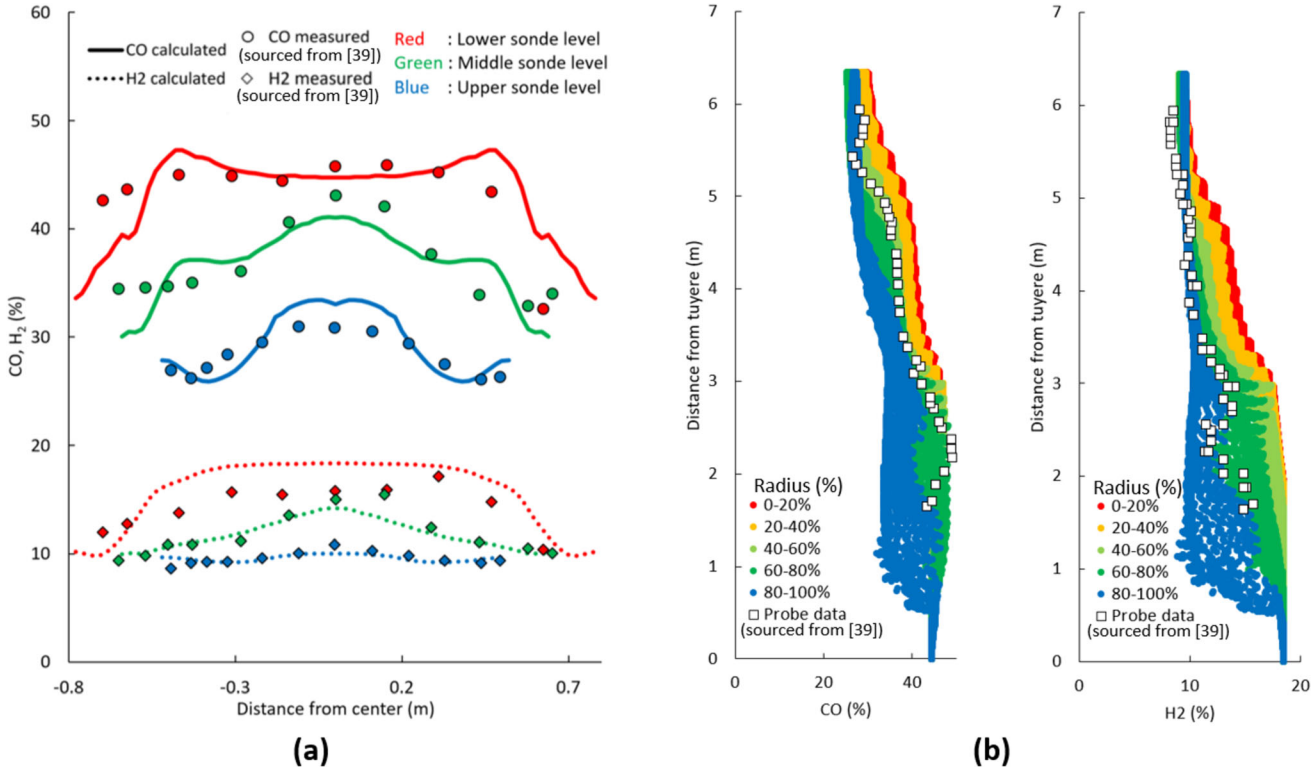


Fig. 4—Comparison of predicted CO and H_2 concentrations with measurements from (*a*) horizontal probes and from (*b*) a vertical probe.

IV. RESULTS

A. *Operating Conditions*

This study explores four configurations of the EASyMelt concept, each incorporating dry reforming and plasma heating, providing a comprehensive comparison with conventional blast furnace operation. Figure 5 outlines the operating conditions for each scenario, which are summarized as follows:

(a) Conventional BF: Standard BF operation, running with hot blast, high PCI rate, and supplemental cold O_2 injection.
(b) NG + COG EASyMelt: This implementation emphasizes reforming of NG and COG without reliance on green energy vectors.
(c) H_2 EASyMelt: This configuration involves the partial replacement of NG and COG with pure hydrogen to enhance the decarbonization potential. It is designed for deployment at steelmaking facilities where large-scale, economically viable renewable electricity is readily available.
(d) NH_3 EASyMelt: Considering the projected economic benefits of using ammonia as a hydrogen transport vector, this scenario substitutes pure hydrogen with cracked ammonia as a green energy source. Although this configuration closely resembles the H_2-based EASyMelt scenario, the gas in the system will have a significantly higher concentration of N_2.
(e) NH_3 + HBI EASyMelt: Building on the previous configuration, this scenario introduces the use of HBI charging as an additional decarbonization means.

To facilitate a more consistent comparison, other key operating parameters such as production rate, composition of reducing agents, or composition of HM were held constant. A detailed overview of these conditions is provided in Table III. Furthermore, the charging strategy was maintained across all scenarios, with only the thickness of the ore layers adjusted to reflect variations in coke rate. In practice, each scenario would require adjustments to the charging program to optimize overall performance; however, this level of operational refinement is outside the scope of this work. To account for energy losses in the piping and injection systems, the syngas exiting the reformer at 1450 °C is considered to reach the plasma torch at 1400 °C, while the syngas cooled to 1000 °C for shaft injection was considered to enter the furnace at 950 °C.

The chemical and thermal efficiencies of the dry reformers and the plasma torches were set according to pilot plant data obtained by Paul Wurth S.A., which cannot be disclosed here due to confidentiality constraints.

B. *Key Performance Indicators*

To evaluate how each scenario affects blast furnace performance, key performance indicators are summarized in Table IV.

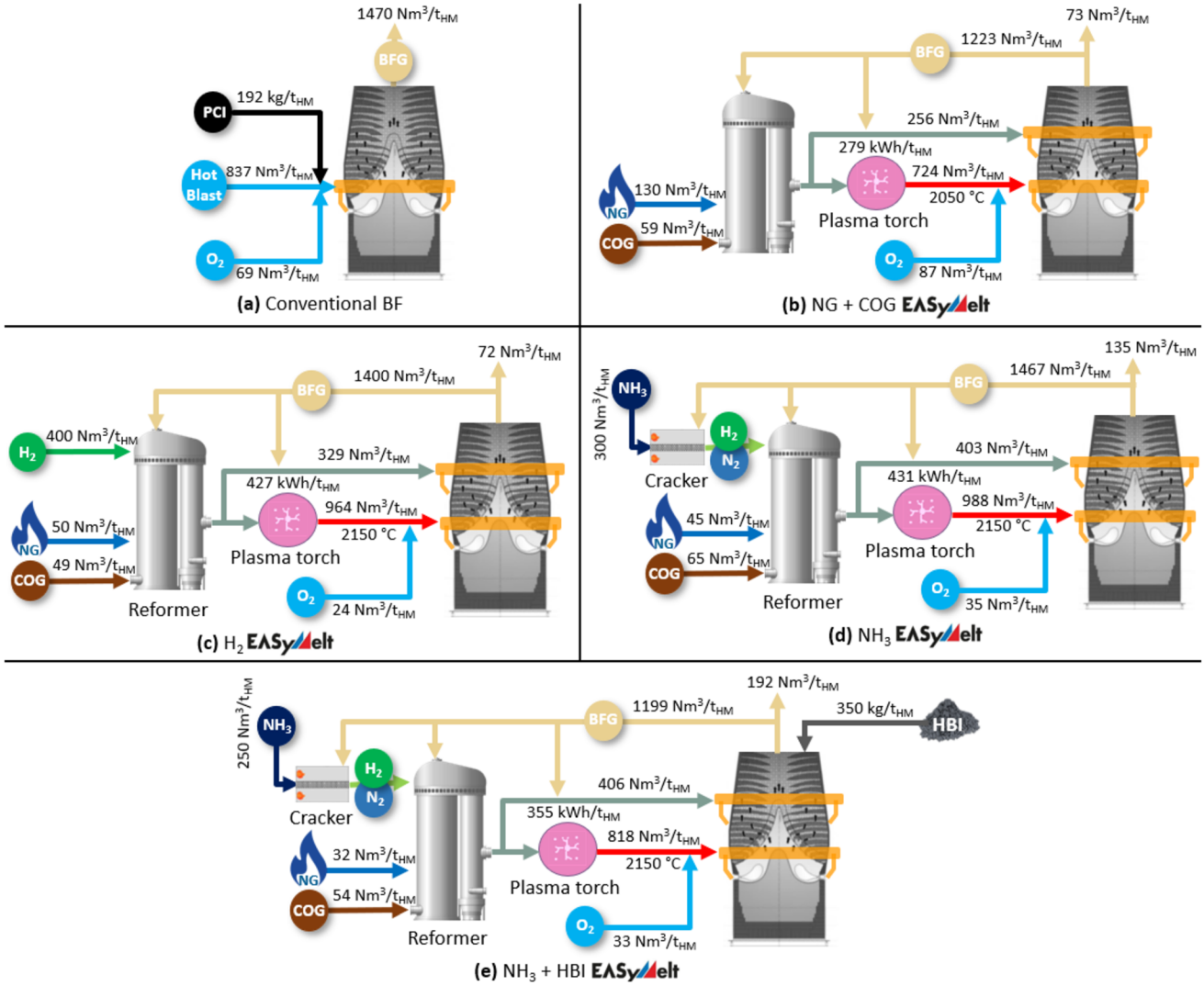


Fig. 5—Operating conditions of tuyere and shaft injection for the different operating scenarios.

Coke rates are first presented, as coke represents the primary source of carbon input in the furnace and is therefore the major contributor to CO_2 emissions. The implementation of EASyMelt is seen to enable a substantial reduction in coke rate. The introduction of NG and COG lowers the coke consumption from 302 to 206 kg/t_{HM}. Further addition of H_2 or cracked NH_3 reduces it even more to 155 and 164 kg/t_{HM}, respectively. Finally, charging HBI brings the coke rate down to 143 kg/t_{HM}. Simultaneously, PC injection, another major source of carbon input in the furnace, is eliminated in all EASyMelt scenarios. It should be noted that the reported coke rates are not intended to represent the absolute minimum achievable. Instead, they reflect values reached while aiming to maintain process stability, optimize fuel utilization, and ensure economic feasibility alongside with CO_2 emission reductions. The main criteria used to ensure process stability were maintaining the top gas temperature above 115 °C to prevent condensation and delayed reduction, keeping the hot-metal temperature within 5 °C of the reference case, and limiting the flame temperature to below 2300 °C. A further, more qualitative, criterion concerns the cohesive-zone geometry, which should maintain an adequate number of coke windows to guarantee effective gas distribution.

To understand gas utilization in the furnace, η_{CO} and η_{H_2} are reported. To ensure comparability with conventional operation, these values are corrected to exclude the CO_2 and H_2O in the top gas that originate directly from shaft injection. Overall, these factors tend to decrease slightly in EASyMelt due to the increase in the amount of CO and H_2 in the furnace. This highlights the key role of top gas recycling in the furnace to effectively use the significant amount of H_2 and CO leaving the BF in the top gas. HBI charging is found to lead to a significant decrease in CO and H_2 utilization. This is due to the substantial portion of the reduction now occurring outside the furnace, while sufficient gas must still be introduced in the furnace to maintain proper thermal conditions. A slight decrease in top gas temperature is observed in the EASyMelt scenarios, as the heat

Table III. Operating Conditions for the Different Scenarios

	Parameters	Value
Hot Metal	production rate (t/d)	7205
	main components (pct)	Fe 94.8; C 4.5; Si 0.4
Iron Ores	ore repartition (pct)	sinter 80; Pellet 20 (conventional) pellet 100 (EASyMelt)
	total Fe and FeO in sinter (pct)	Fetot 56.3; FeO 8.5
	sinter moisture (pct)	0.1
	total Fe and FeO in pellet (pct)	Fetot 66.1; FeO 0.88
	pellet moisture (pct)	1.3
Reducing Agents	coke main components (pct)	C 88.5; Ash 10.1
	coke moisture (pct)	5
	coal main components (pct)	C 79.4; Ash 9.2
	COG main components (vol-pct)	CO 9; CO_2 3; H_2 57; C_nH_m 25.2; N_2 5.5
	NG main components (vol-pct)	CO_2 0.6; C_nH_m 99.4
	cracked ammonia components (vol-pct)	H_2 75; N_2 25
	HBI main components (pct)	Femet 87; FeO 7
Top Conditions	burden temperature (°C)	10
	top gauge pressure (10^5 Pa)	1.7
BF Characteristics	working volume (m^3)	2934
	number of tuyeres	32
	hearth diameter (m)	12
	distance tuyere to shaft injection (m)	8.9

The shares are expressed in mass-pct unless otherwise stated.

Table IV. Key performance Indicators of the Different Operation Scenarios

	Conventional	NG + COG EASy-Melt	H_2 EASy-Melt	NH_3 EASy-Melt	NH_3 + HBI EASy-Melt
Coke Rate (kg/t_{HM})	302	206	155	164	143
PCI Rate (kg/t_{HM})	192	0	0	0	0
Total Carbon Rate (kg/t_{HM})	428	270	177	185	157
η_{CO}(Pct)	48.8	48.7	36.2	35.6	28.7
η_{H_2}(Pct)	36.0	30.4	33.9	36.2	25.4
Top Gas H_2 (Pct-dry)	4.5	30.8	51.3	43.1	48.7
Top Gas CO (Pct-dry)	25.1	33.8	29.5	21.6	21.2
Top Gas CO_2 (Pct-dry)	23.9	34.8	18.5	13.3	9.7
Top Gas H_2O (Pct)	4.0	13.5	22.3	20.8	15.4
Top Gas Temperature (°C)	178	116	119	153	135
Reduction Degree Solid State (Pct)	73	95	92	87	91
HM Temperature (°C)	1477	1482	1473	1481	1482
Flame Temperature (°C)	2264	2286	2053	2233	2256
Heat Loss (MJ/t_{HM})	391	360	400	408	386

contribution from the shaft gas does not fully offset the effects of the reduced coke rate (*i.e.*, larger share of ore in the burden) and the increased share of endothermic hydrogen reduction. Still, the top gas temperature remains within an acceptable range for safe and stable BF operation. Notably, even with the increased water content in the gas, the dew point remains consistently well below the top gas temperature across all cases. In the worst-case scenario (c), with 22.3 pct H_2O in the top gas, the calculated dew point is approximately 86 °C, which is still significantly lower than the predicted top gas temperature. An additional performance indicator, *i.e.*, the reduction degree in the solid state, is finally presented. As the name suggests, this metric indicates the reduction degree reached by the ferrous burden while still in the solid state. The remaining reduction takes place during the so-called final reduction stage, where FeO is reduced in the liquid phase. As the final reduction is strongly endothermic and directly consumes carbon, this indicator provides valuable insight into the efficiency and sustainability of the process. Overall, the strong reducing power of the syngas used in EASyMelt implementations leads to a notable increase in the solid-state reduction degree. The highest reduction degree is achieved in the scenarios using NG, COG, and H_2, as the resulting syngas consists almost entirely of the reductants H_2 and CO. The use of cracked NH_3 results in a slight decrease in the reduction

degree, as the presence of N_2 in the syngas marginally dilutes its reducing potential. Nevertheless, the achieved reduction degree of 87 pct remains significantly higher than that of conventional operation, which stands at 73 pct. Finally, charging HBI leads to a modest increase in the overall reduction degree, as a significant portion of the reduction has already been carried out externally prior to furnace entry.

For a more in-depth analysis, Figure 6 provides a detailed breakdown of carbon input sources in the blast furnace across the different scenarios, serving as a strong indicator of the CO_2 emissions intensity of the processes. The carbon input rate decreases from 428 kg/t_{HM} for conventional operation down to 270 kg/t_{HM} for EASy-Melt with NG + COG. This reduction is attributed to the lower coke consumption and the elimination of PCI. The addition of H_2/cracked NH_3 further lowers carbon input to 177 and 185 kg/t_{HM}, respectively, due to a further decrease in the coke rate and a lower amount of NG and COG required. Finally, HBI charging reduces the total carbon input to 157 kg/t_{HM}. The observed decrease in coke rate can be attributed primarily to two key mechanisms. First, the better reduction discussed above (cf. Table IV) leads to a lower coke consumption for the final reduction. Second, with the replacement of hot blast by syngas, less O_2 is introduced at the bosh tuyere, resulting in less coke combustion. Instead, the necessary thermal energy for the furnace operation is supplied by syngas heated using the plasma torches.

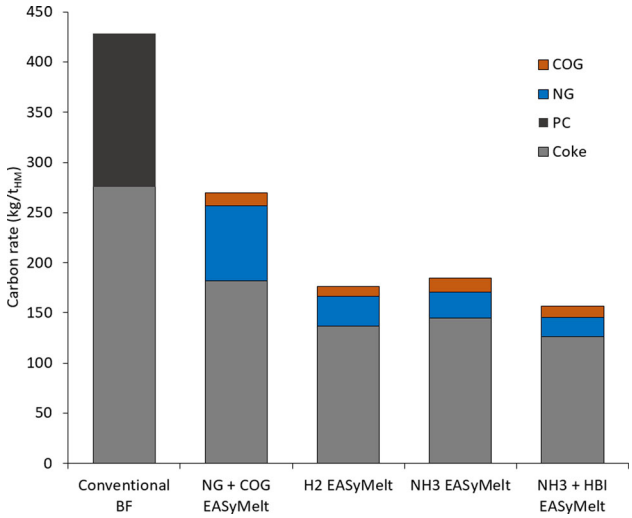


Fig. 6—Carbon input sources in the BF under the different scenarios.

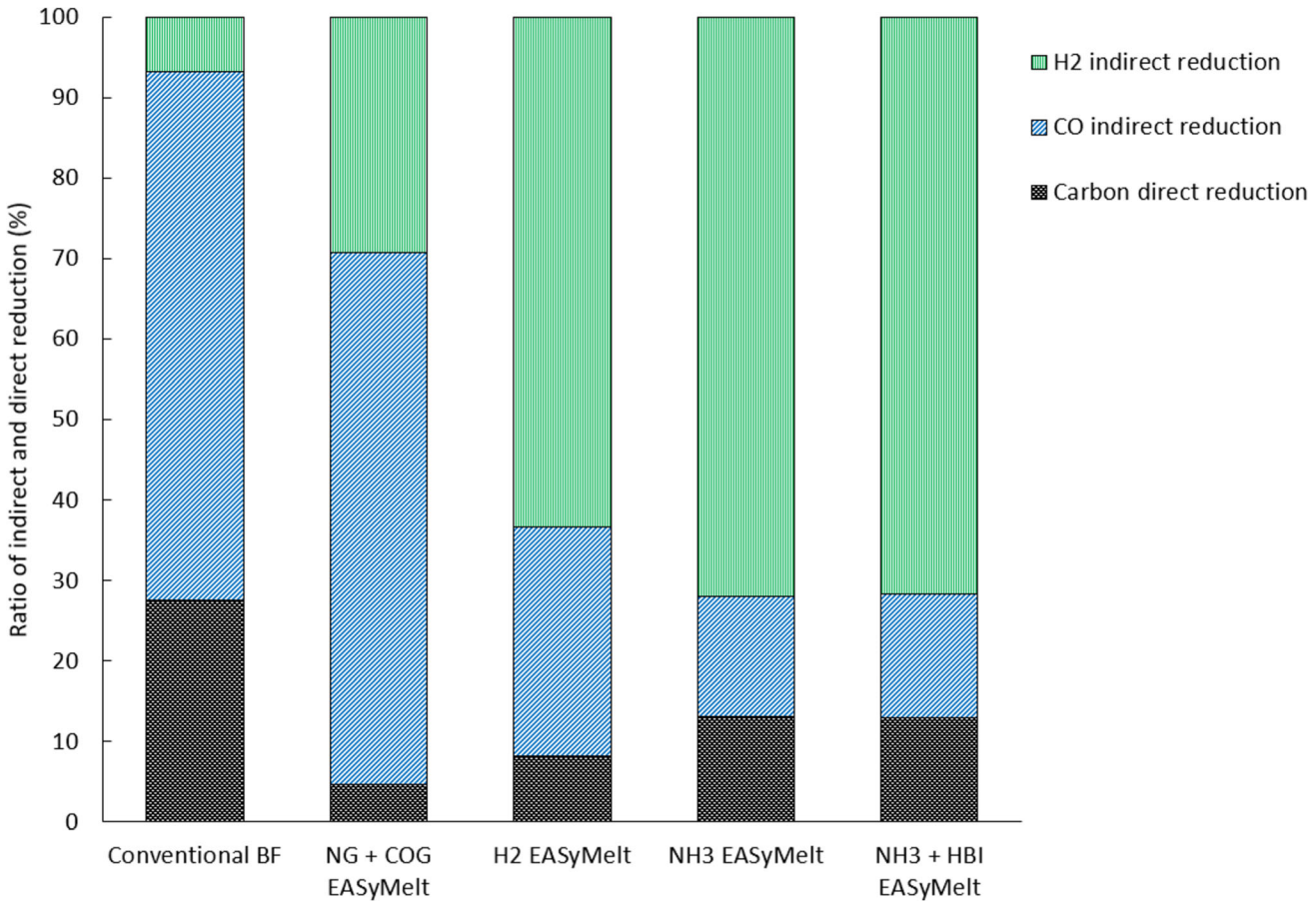


Fig. 7—Repartition of reduction mechanisms occurring in the BF under the different scenarios.

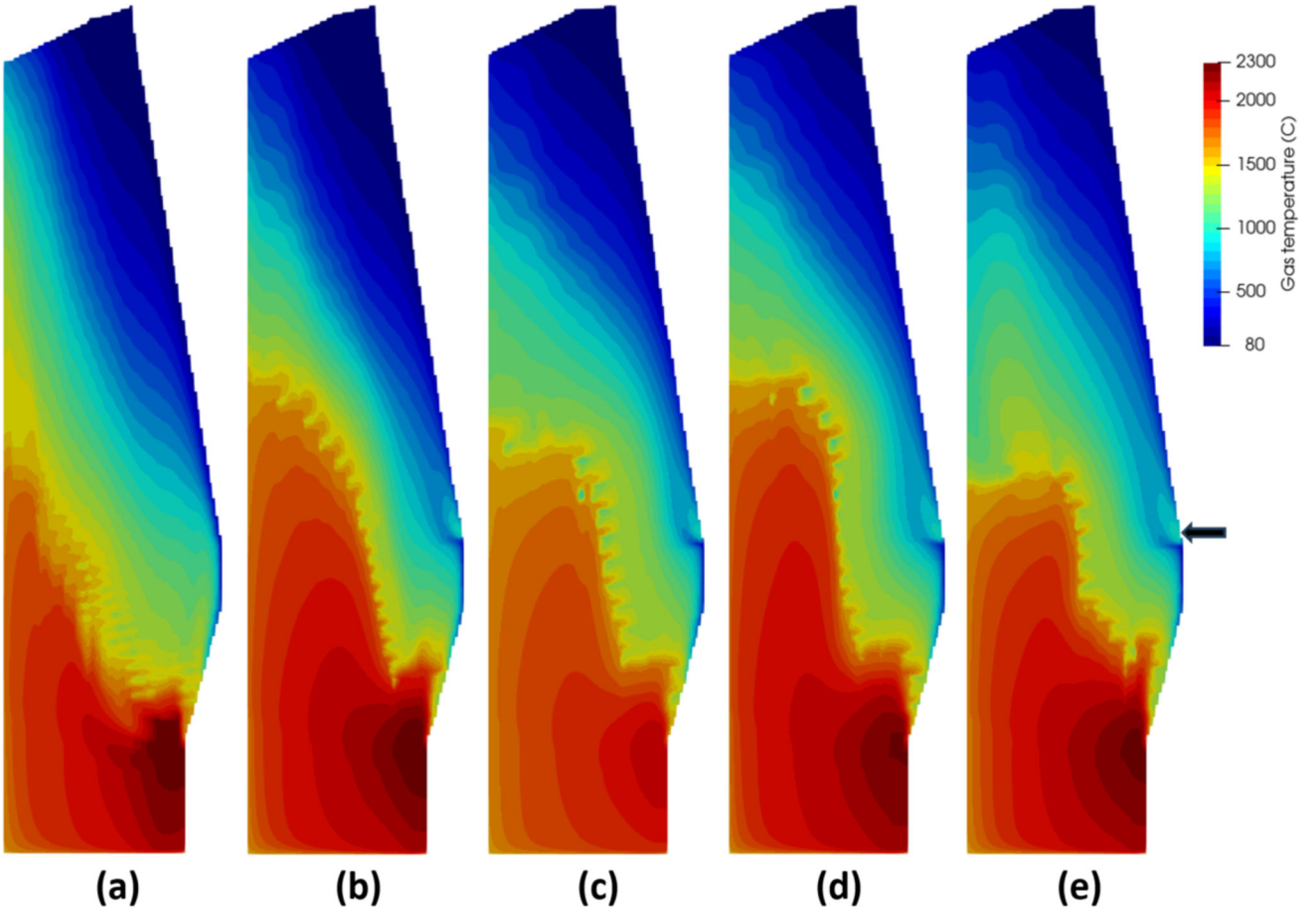


Fig. 8—Gas temperature distribution of (*a*) Conventional BF, (*b*) NG + COG EASyMelt, (*c*) H_2 EASyMelt, (*d*) NH_3 EASyMelt and (*e*) NH_3 + HBI EASyMelt.

To better illustrate the changes in reduction phenomena within the furnace, Figure 7 shows the proportion of each reduction mechanism inside the BF for the respective processes. As anticipated, the share of direct reduction involving the reaction of liquid FeO with solid carbon decreases in the EASyMelt cases. This is consistent with the higher solid-state reduction degree reported in Table IV. For case (e) with the use of HBI, a significant part of the reduction now occurs externally, and the burden enters the furnace with an average reduction degree around 35 pct. As a result, even if the distribution of reduction mechanisms appears nearly identical between scenarios (d) and (e), the absolute amount of reduction occurring inside the furnace is lower in scenario (e).

Regarding indirect reduction by CO and by H_2, a marked increase in H_2-based reduction is observed as the hydrogen input to the furnace rises and CO availability decreases. In conventional blast furnace operation, hydrogen makes up only a small fraction, approximately 8 pct, of the tuyere gas. While it contributes to the reduction of iron oxides, its role remains secondary to the dominant indirect reduction by carbon monoxide. With the implementation of the EASyMelt process, hydrogen input increases significantly. In case (b), hydrogen represents about 40 pct of the tuyere gas, rising to 65 pct in case (c) with the addition of pure H_2. This is accompanied by a pronounced increase in the share of H_2 indirect reduction. In cases (d) and (e), although the hydrogen concentration is slightly lower than in case (c) due to the added cracked ammonia containing 25 pct nitrogen, the ratio H_2/CO is even higher (from 1.9 to 2.5). Consequently, the proportion of H_2 indirect reduction becomes even greater.

C. *Internal State*

For gaining a deeper understanding on the EASyMelt process, the internal state of the furnace for the different concepts is presented and analyzed.

The thermal state of the furnace is first illustrated in Figure 8, which presents the gas temperature distribution. With the energy supplied by the plasma torches and less required final reduction, a proper thermal state in the lower part of the furnace can be effectively maintained for the EASyMelt scenarios. The effect of shaft injection is clearly seen in elevated temperatures around the injection point (indicated by an arrow in the rightmost panel). Compared to conventional operation, shaft injection promotes a more uniform temperature distribution within the furnace, decreasing the

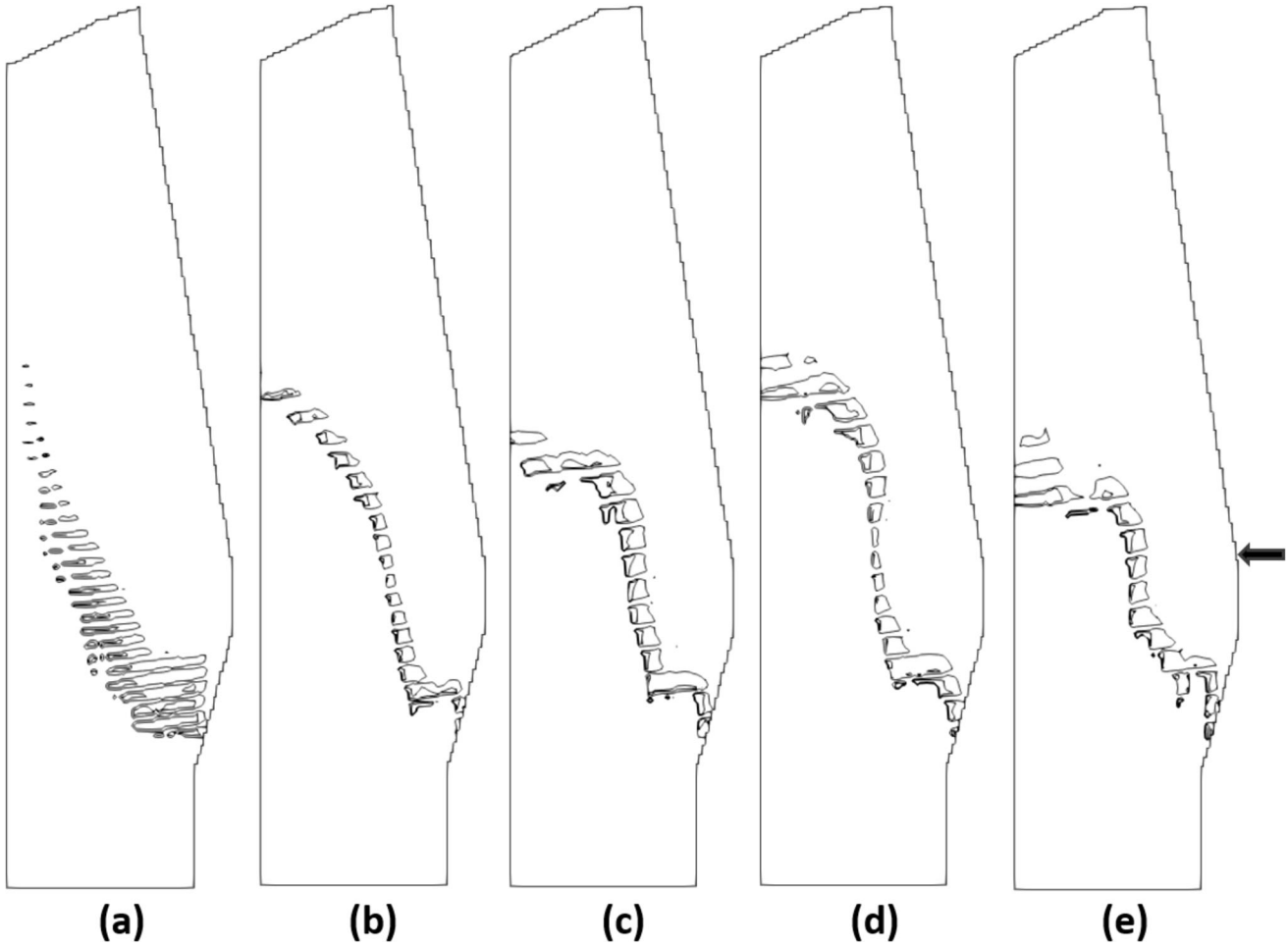


Fig. 9—Cohesive zone shape represented by porosity contours of (*a*) Conventional BF, (*b*) NG + COG EASyMelt, (*c*) H_2 EASyMelt, (*d*) NH_3 EASyMelt and (*e*) NH_3 + HBI EASyMelt.

temperature gradient between the center and the wall. This more balanced thermal profile reduces thermal stress on the bell-less top® charging system located above the furnace center. Another key indicator of the thermal state of the furnace is the cohesive zone shape, as illustrated in Figure 9 using a porosity contour. The figure also delineates the transition between the softening region of CZ, where the solid burden starts softening, and the melting region where the material is fully liquefied before dripping down. A notable observation is that the cohesive zone is thinner in all EASyMelt scenarios compared to conventional operation, with in particular a narrower melting region. Similar findings have been reported in other studies at increased hydrogen input in the tuyeres,[13,41] attributed to the reduced heat demand of the direct reduction reaction and the increased solid reduction degree which leads to a narrower temperature range of the melting zone.[42] A thinner CZ reduces the pressure drop over the CZ, enhancing furnace permeability. The root of the CZ is seen to be slightly higher in the EASyMelt cases as a result of the thermal energy brought by the shaft gas. When it comes to the height of the CZ at the center of the furnace, cases (b) and (d) exhibit elevated levels, nearly matching those observed during conventional operation. This is primarily due to the reduced heat consumption by direct reduction and the additional heat supplied by the plasma torches, which enables the attainment of high flame temperatures. On the other hand, cases (c) and (e) show a lower CZ position at the furnace center. In case (c), which involves hydrogen addition, this is primarily due to a lower flame temperature, caused by a higher amount of top gas recycling which leads to more CO_2 and H_2O in the syngas. Indeed, more BFG is available compared to (d) and (e), since it is not needed for ammonia cracking. On the other hand, less NG gas is used than in (b), lowering the need of CO_2 for reforming CH_4. This higher amount of recycling is still desirable to reduce requirement of relatively expensive hydrogen. For case (e), involving HBI charging, a similar trend has been observed by Kobe Steel during their recent test campaign on massive HBI charging in a conventional blast furnace.[25] Still, the shape of the CZ appears acceptable across all cases, each incorporating a comfortable number of coke layers that allow for proper distribution of the bosh gas. It should be noted that in the current study the same charging strategy was maintained, only changing the ore-to-coke ratio

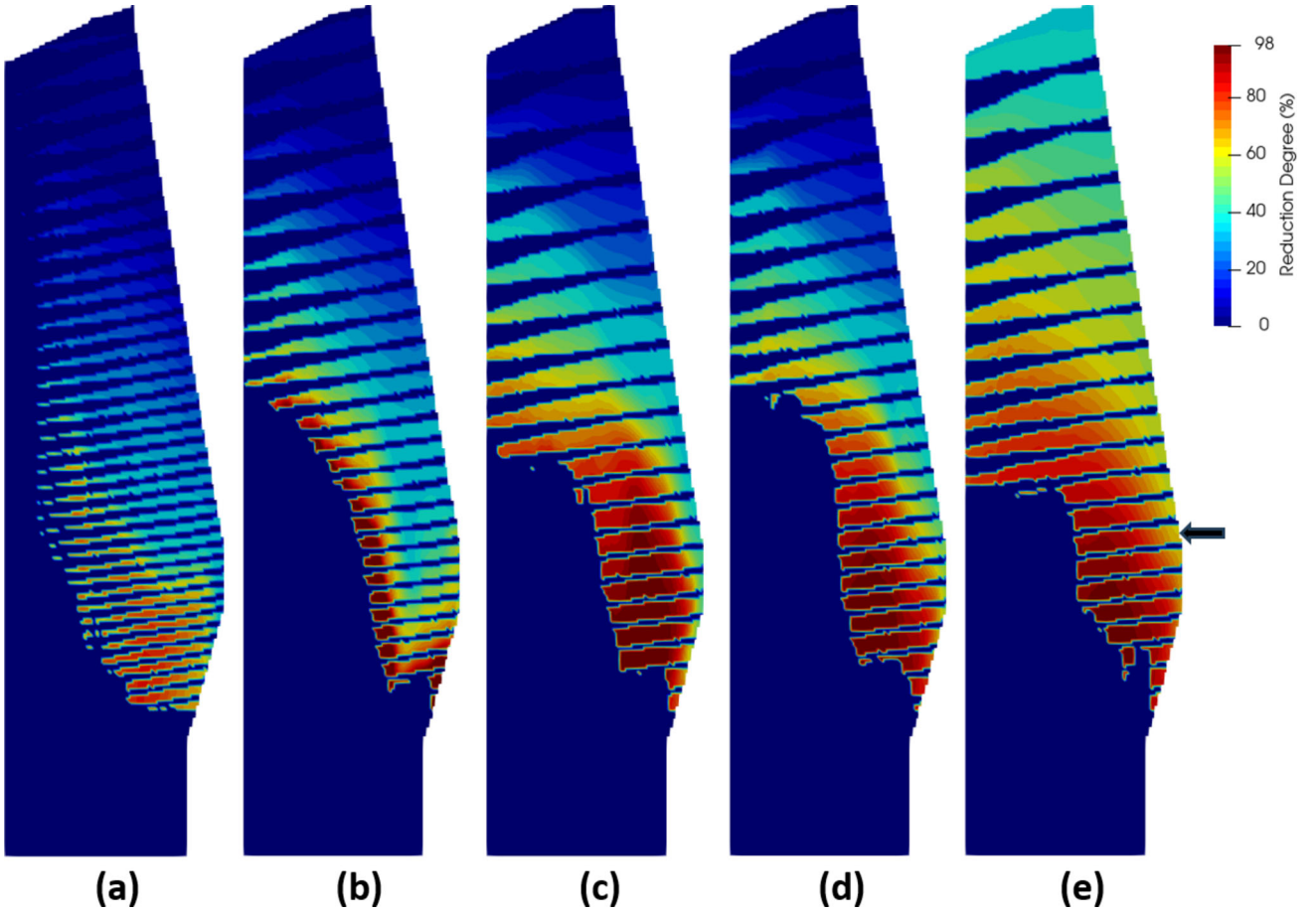


Fig. 10—Reduction degree distribution of (*a*) Conventional BF, (*b*) NG + COG EASyMelt, (*c*) H_2 EASyMelt, (*d*) NH_3 EASyMelt and (*e*) NH_3 + HBI EASyMelt.

depending on the predicted coke rates. In practice, the charging program will be changed for each scenario to optimize overall process performance.

The reduction behavior is illustrated in Figure 10 through the distribution of the reduction degree. The significantly higher reduction degree observed upon reaching the dripping zone across all EASyMelt scenarios is clearly observed. Case (c) or (d) exhibits a broader region of high reduction degree, where FeO is largely reduced, compared with case (b). This results from the higher hydrogen content in the ascending syngas, which is a faster reductant at these lower temperatures, together with the longer persistence of elevated gas temperatures above the cohesive zone, as observed in Figure 8. The impact of charging HBI is also clearly seen: while the reduction degree at the top of the furnace is around 3 pct for all other cases, it is 35 pct in case (e) since part of the reduction now occurs externally, prior to charging.

The spatial distribution of gas velocity magnitude is presented in Figure 11. The influence of the previously discussed thinner CZ and the lower tuyere gas volume are clearly visible. In conventional operation, the high pressure drop over the CZ and relatively high amount of tuyere gas results in elevated gas velocities in and downstream of the coke windows. In contrast, under EASyMelt conditions, noticeably lower gas velocities in these regions can be observed. Additionally, gas injection at the shaft level contributes to a more uniform velocity distribution, significantly reducing the disparity between central and peripheral gas flow.

To illustrate the changes in gas composition within the blast furnace under the different scenarios, the distributions of hydrogen and carbon monoxide are presented in Figures 12 and 13. By showing how H_2 and CO are produced and consumed inside the furnace, these gas distributions offer a more complete picture of the reduction repartition presented in Figure 8. Furthermore, the impact of shaft injection on the gas composition can be observed. However, the figure may give the misleading impression that only a tiny region of the furnace is affected by the shaft gas. To clarify this, in case (e), the shaft gas penetration is found to be about 1.1 m at the injection point, where the furnace radius is 7 m. This indicates that almost 30 pct of the furnace cross-sectional area is influenced by the shaft gas, demonstrating a much more substantial effect than the figure might imply. Despite adequate penetration, hydrogen from the shaft gas consistently shows lower utilization compared to hydrogen from the tuyere gas across all scenarios. This is evident from the higher hydrogen concentrations observed near the furnace wall.

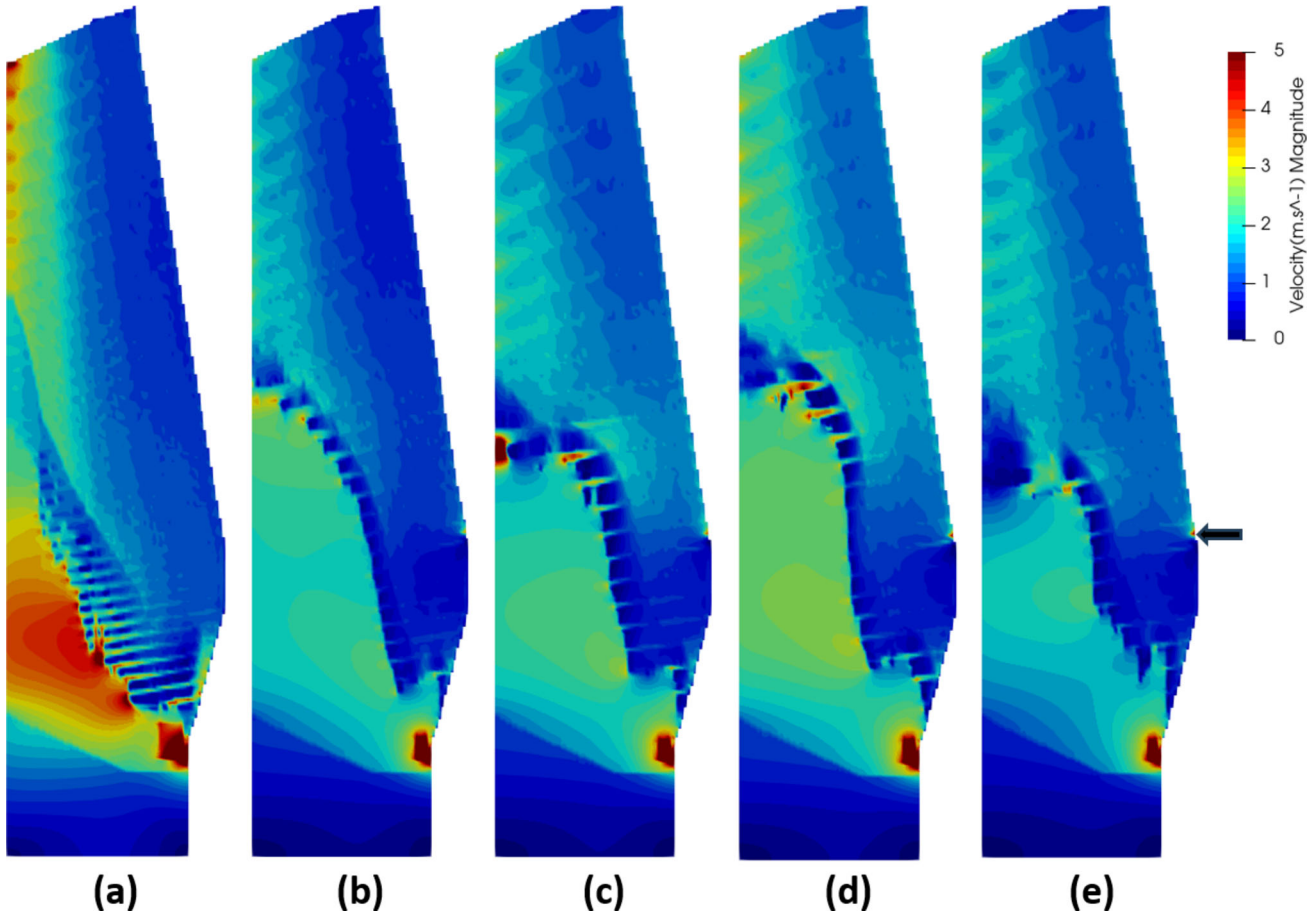


Fig. 11—Gas velocity magnitude distribution of (*a*) Conventional BF, (*b*) NG + COG EASyMelt, (*c*) H_2 EASyMelt, (*d*) NH_3 EASyMelt and (*e*) NH_3 + HBI EASyMelt.

Two main factors contribute to the lower efficiency. First, to maintain process stability, the shaft gas is injected at a relatively low temperature of around 950 °C, which limits the thermal energy available for the endothermic reduction reactions involving hydrogen. Second, to achieve this lower temperature, high-temperature syngas (at about 1400 °C) from the syngas reformers is mixed with top gas. This dilution results in a gas mixture with lower reducing potential, as it contains higher concentrations of H_2O and CO_2. The reduction potential of the shaft gas is then not significantly higher than that of the ascending gas, simplifying operation by minimizing asymmetry in the system. Overall, the marginally lower gas utilization highlights that the shaft gas injection not only supports the iron oxide reduction but also serves to provide sufficient thermal energy to the shaft for heating the burden (thus giving rise to a sufficiently high top gas temperature).

D. *Energy Consumption, CO_2 Emissions, and OPEX of Crude Steel Production*

To provide a more comprehensive assessment of EASyMelt's impact, the energy consumption, OPEX, and CO_2 emissions of crude steel production at the integrated steel plant are investigated for each scenario. Figure 14 outlines the boundaries of the steel plant considered in this analysis, detailing the relevant inputs, outputs, and processing units involved in crude steel production. The scope of the study does not extend beyond the BOF, as the downstream processes producing the final steel product vary significantly depending on each plant's specific requirements for steel properties, quality, and final product form. Still, to get an accurate representation of the typical energy usage of an integrated steel plant, a provision of 1.3 GJ/t_{Cs} from internal steel plant gases was included in all cases to account for reheating and rolling.

Figure 15(a) illustrates the different sources and quantities of energy inputs for crude steel production at the integrated steel plant, under the assumption that no electricity is generated on-site and export gas is considered instead. In conventional operations, the gross energy consumption at the steel plant amounts to 18.6 GJ/t_{Cs}, with a net energy consumption of 15.1 GJ/t_{Cs}, while the remainder is available for export, as a low calorific steel plant off-gas and coke making oils. A majority of this energy input is derived from coal, a high-emission energy source. In contrast, all EASyMelt scenarios exhibit significantly less energy available for export, only around 0.3 GJ/t_{Cs}, primarily in the form of tar produced by the coke oven plant. The first three

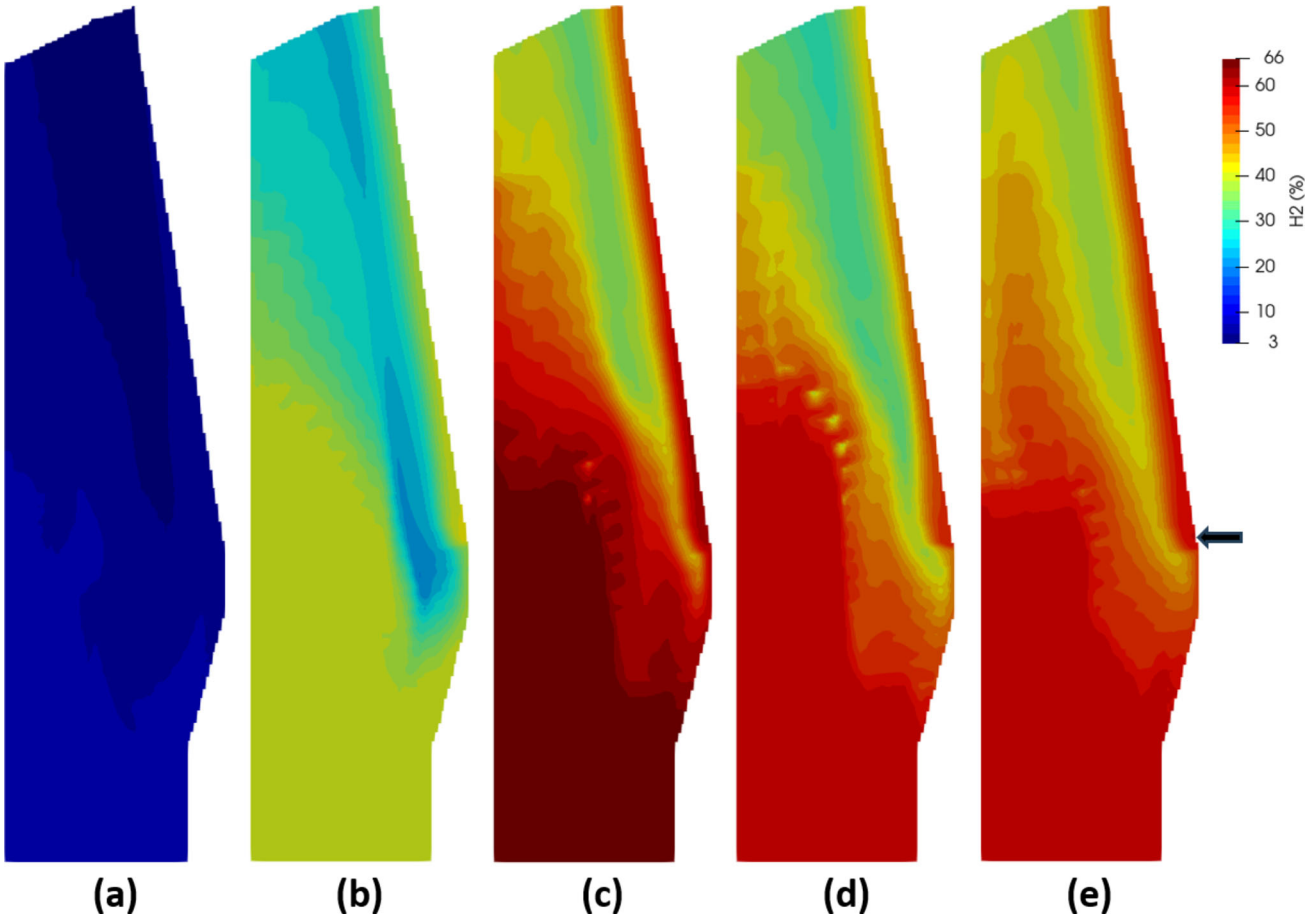


Fig. 12—H_2 distribution of (*a*) Conventional BF, (*b*) NG + COG EASyMelt, (*c*) H_2 EASyMelt, (*d*) NH_3 EASyMelt and (*e*) NH_3 + HBI EASyMelt.

EASyMelt cases have nearly identical energy consumption at about 13.2 GJ/t_{Cs}. The decrease compared to conventional BF operation is explained by the lower coke rates, meaning lower amount of energy consumed at the coke oven plant, and the omission of the sinter plant, which is also an energy consumer. The H_2 EASyMelt scenario offers a marginal advantage of 0.1 GJ/t_{Cs} attributed to a lower coke rate and the elimination of ammonia cracking; this difference is negligible in practical terms. When HBI charging is implemented, the energy consumption drops to 10.6 GJ/t_{Cs}, due to the external reduction of HBI. Overall, the transition from conventional to EASyMelt processes marks a clear shift away from coal dependency toward energy sources with lower carbon footprint, such as natural gas, electricity, and, in advanced cases, renewable carriers like hydrogen, ammonia, and HBI.

In general, steel plant off-gas is not readily exportable. Instead, steelmakers maximize its internal utilization, with any surplus typically converted into electricity at an on-site power plant. Figure 15(b) illustrates such a case, where all remaining off-gas is used for power generation. These power plants, however, operate at relatively low efficiency, assumed here to be 35 pct. As a result, under this assumption, the energy demand for crude steel production in conventional operation rises to 17.1 GJ/t_{Cs}. In contrast, the EASyMelt scenarios show only a marginal increase in energy use, since hardly any gas was left for export. This highlights that recycling steel plant off-gas or integrating it into other processes is generally more efficient and beneficial than converting it to electricity.

To assess both environmental and economic impacts of the different EASyMelt scenarios, Figure 16 presents the changes in crude steel production OPEX relative to that of the conventional operation for different CO_2 emission penalty levels, as a function of the projected scope 1 + 2 CO_2 emissions reduction. The underlying numbers for this analysis, chosen to be representative of a steel plant in Europe, are presented in Table V. Given the extremely limited availability of hydrogen, ammonia, and HBI in Europe at present, the assumed figures necessarily rely on projections and should be interpreted as optimistic forward-looking prices. A plausible pathway to achieving such price levels is the production of green hydrogen in regions with abundant, low-cost renewable energy, followed by the transport of the different hydrogen carriers to the steel plant, as discussed in Section II.

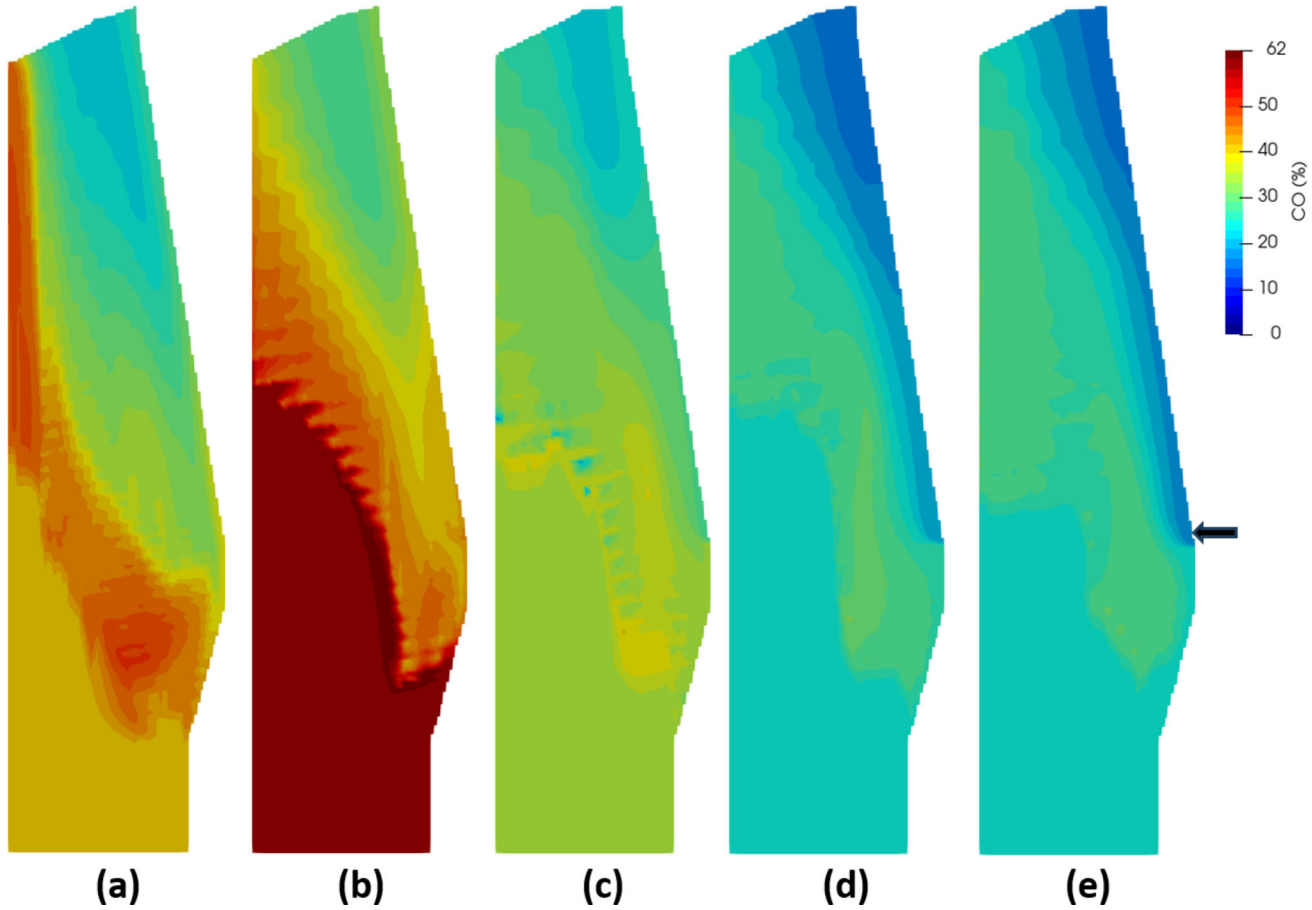


Fig. 13—CO distribution of (*a*) Conventional BF, (*b*) NG + COG EASyMelt, (*c*) H_2 EASyMelt, (*d*) NH_3 EASyMelt and (*e*) NH_3 + HBI EASyMelt.

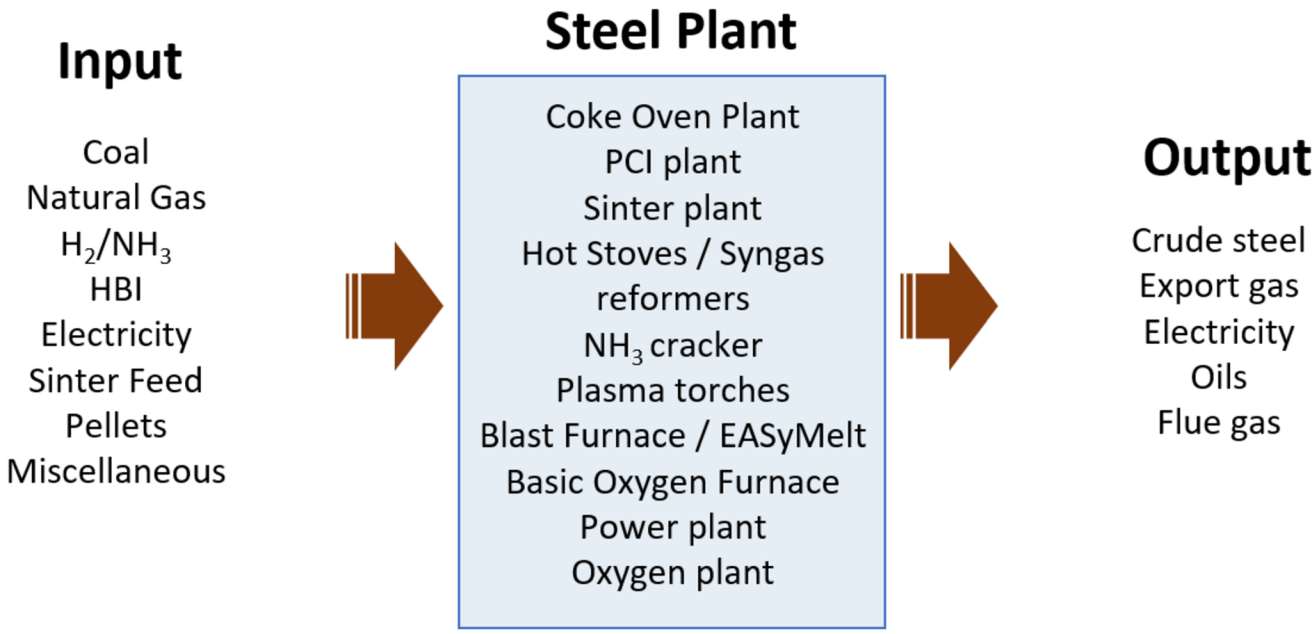


Fig. 14—Boundaries considered at steel plant for crude steel production.

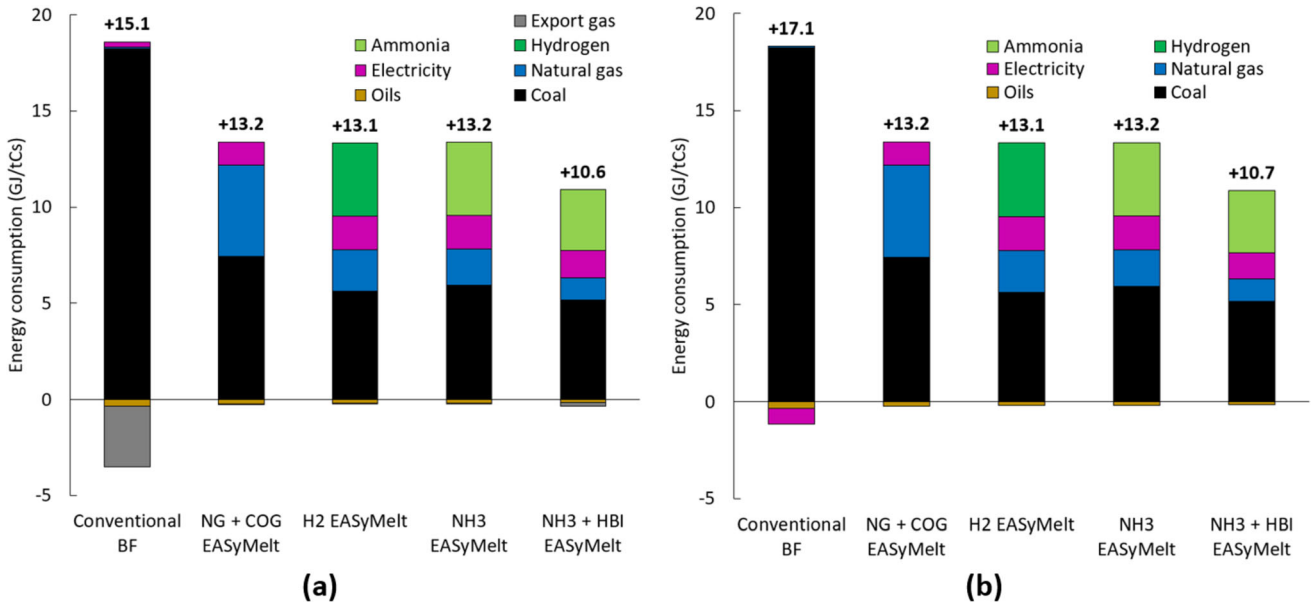


Fig. 15—Sources of energy at the steel plant for crude steel production of the different scenarios in case where (*a*) no electricity is generated on-site and (*b*) all remaining steel plant off-gas is converted to electricity.

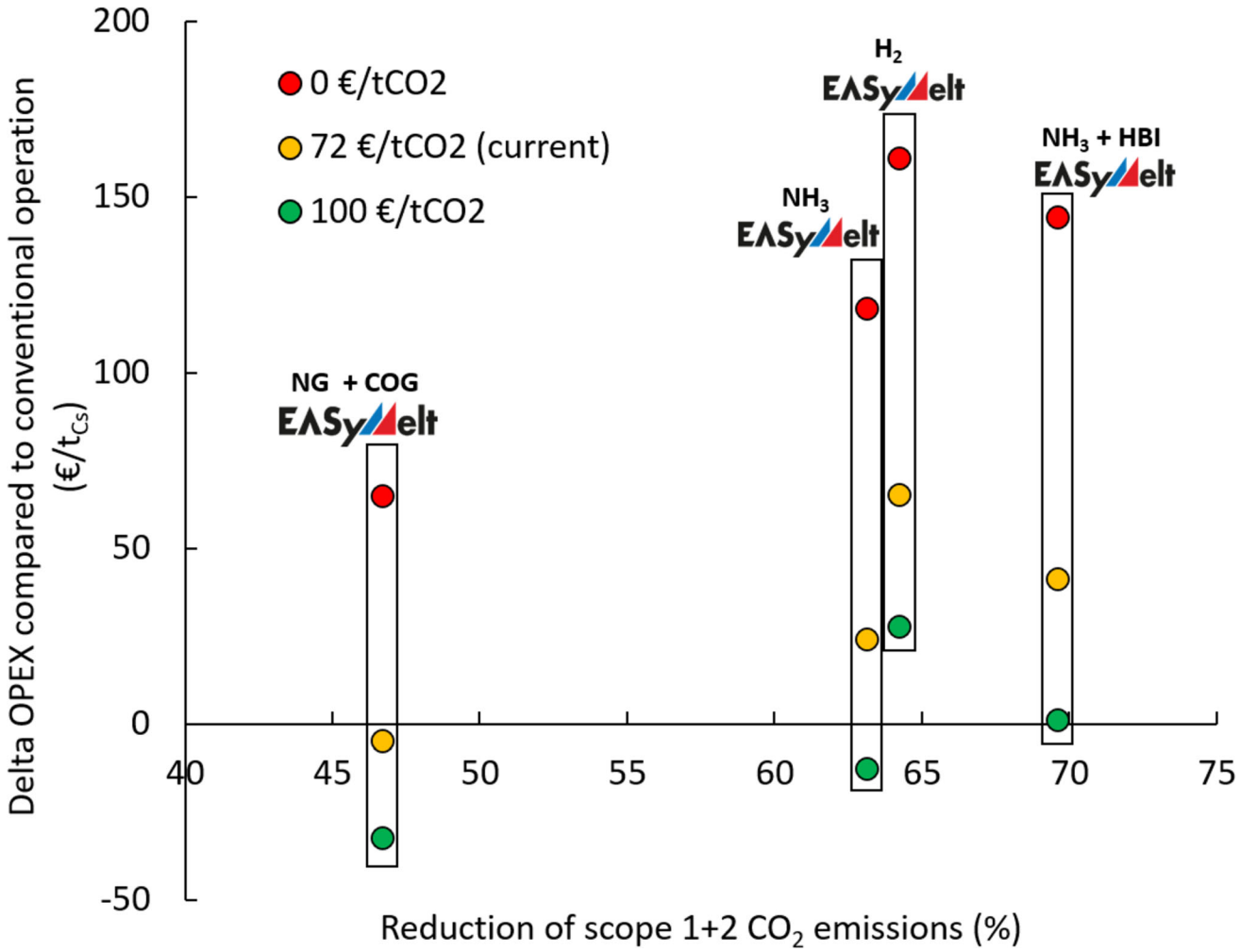


Fig. 16—CO_2 emissions reduction and ΔOPEX of crude steel production for the different scenarios compared to conventional operation.

Table V. Central Values Used for the CO_2 and OPEX Assessment Presented in Fig. 16

Coking Coal Price (€/t)	231	ore fines price (€/t)	123
Coke Oven Plant Emissions Scope 1 + 2 (kg_{CO2}/t_{coke})	345	sinter plant emissions scope 1 + 2 (kg_{CO2}/t_{sinter})	271
Electricity Price (€/MWh)	90	HBI price (€/t)	420
Electricity Scope 2 (kg_{CO2}/GJ)	22	pellet price (€/t)	175
PCI Coal Price (€/t)	128	BOFG price (€/GJ)	7.5
PC plant Emissions Scope 1 + 2 (kg_{CO2}/t_{PC})	2	BOF plant emissions scope 1 + 2 (kg_{CO2}/t_{Cs})	143–152*
COG Price (€/GJ)	7.5	compressed air price (€/t)	11
NG Price (€/GJ)	9	compressed air scope 2 (kg_{CO2}/Nm^3)	0.01
Ammonia Price (€/GJ)	20	O_2 price (€/t)	47
Hydrogen Price (€/GJ)	30	O_2 plant scope 1 + 2 (kg_{CO2}/Nm^3)	0.04
BFG Price (€/GJ)	6		

*Higher BOF plant emissions for EASyMelt cases as no off-gas left for low-efficiency electricity generation which is replaced by external electricity.

Due to its higher coke rate and the absence of green energy input, the NG + COG EASyMelt scenario is found to achieve the lowest CO_2 emissions reduction among the scenarios evaluated, still reaching a notable 47 pct reduction. On the other hand, this scenario requires the lowest CO_2 price to achieve net OPEX savings and is already economically viable under the current EU ETS carbon price, which is about 72 €/t_{CO2} in the first half of 2025.[43] The addition of H_2 or cracked NH_3 enables a further reduction in coke consumption and a decrease in NG usage. Although NG is less carbon-intensive than coal, it remains a significant source of CO_2 emissions. The emissions are reduced by 63 pct in the NH_3-based scenario and by 64 pct in the H_2-based scenario. While hydrogen offers a slight advantage in terms of emission reduction, its higher cost compared to NH_3 negatively impacts costs. OPEX neutrality is only achieved at a carbon price of 121 €/t_{CO2} for the H_2 route, whereas the NH_3-based EASyMelt scenario reaches OPEX neutrality at a lower carbon price, 90 €/t_{CO2}. Finally, the addition of HBI enables 70 pct savings in CO_2 emissions, while having a slightly negative impact on OPEX with neutrality achieved at a carbon price of 101 €/t_{CO2}.

V. CONCLUSIONS

The EASyMelt concept analyzed numerically in this paper brings forward a suite of carbon-saving technologies for the blast furnace, including top gas recycling, plasma heating for direct electrification, gas reforming, two-level parallel injection, and the potential integration of green energy vectors. This advanced approach offers a promising pathway to significantly reduce CO_2 emissions in blast furnace ironmaking. The current work has investigated feasible EASyMelt implementations based on different mixes of COG, NG, H_2, cracked NH_3, and HBI. A multi-fluid blast furnace model was employed to evaluate the impact of the various implementations on the overall process performance and on the internal state of the furnace, compared to conventional blast furnace operation. The study also investigated the effects of the different scenarios on energy demand, CO_2 emissions, and OPEX associated with crude steel production at the steel plant. The key findings are summarized as follows:

1. Carbon input, a key indicator of CO_2 emission intensity, significantly decreased for all EASyMelt scenarios. This is due to the lower coke rates, enabled by top gas recycling, enhanced burden reduction and the heat provided by the plasma torches, as well as the elimination of PCI. The use of NG and COG as lower carbon alternatives also contributes to this carbon input reduction, while the integration of green energy vectors further amplifies the effect.
2. The blast furnace was found to maintain an acceptable top gas temperature across all scenarios, while top gas utilization was generally found to decrease. While such a decline would be problematic in a conventional blast furnace, it is not an issue in the EASyMelt process, where the top gas is either recycled in the furnace or used in high efficiency applications (*e.g.*, heating of the syngas dry reformers, heating of the ammonia cracker…). This results in little BFG left for export to low-efficiency applications like combustion for electricity generation (cf. Figure 15).
3. The internal state of the furnace was analyzed to gain a deeper understanding of the BF behavior under the different EASyMelt scenarios. The thermal conditions were found to remain acceptable in all cases, resulting in a well-formed cohesive zone with sufficient coke windows to ensure a proper gas distribution (cf. Figure 11). Additionally, the improved reduction of the solid ferrous burden (cf. Figure 10) and the drastic increase in H_2 level in the furnace (cf. Figure 12) were clearly demonstrated.
4. A combined environmental and economic assessment showed that the EASyMelt scenario using NG and COG can achieve up to 47 pct CO_2 reduction in crude steel production while also delivering OPEX savings at current European carbon price level. Scenarios involving NH_3 and HBI offer even greater emission reductions, up to 70 pct, but require a higher carbon penalty to be economically viable. While pure H_2 use can yield similar emission reductions as NH_3, its application is only feasible for steel

plants with reliable access to abundant, low-cost renewable energy, which is generally not the case in Europe. In case of intercontinental transport requirement, direct ammonia usage is the clear choice over hydrogen.

The results demonstrate that EASyMelt offers a feasible and flexible pathway for decarbonizing blast furnace ironmaking. An initial implementation using only NG and COG is cost-competitive and offers the adaptability to swiftly incorporate ammonia and/or HBI when economic conditions become favorable. The remaining hard-to-abate emissions of CO_2 could be captured and stored to achieve carbon neutrality. Since this final step addresses only a small fraction of the total emissions, it carries less regulatory risk and is more likely to gain political and societal acceptance than CCS adopted as the sole decarbonization strategy.

ACKNOWLEDGMENTS

The present work is supported by the Luxembourg National Research Fund (FNR) (16659925) and Paul Wurth S.A. The financial support is gratefully acknowledged.

FUNDING

Open access funding provided by Åbo Akademi University.

CONFLICT OF INTEREST

On behalf of all authors, the corresponding author states that there is no conflict of interest.

OPEN ACCESS

This article is licensed under a Creative Commons Attribution 4.0 International License, which permits use, sharing, adaptation, distribution and reproduction in any medium or format, as long as you give appropriate credit to the original author(s) and the source, provide a link to the Creative Commons licence, and indicate if changes were made. The images or other third party material in this article are included in the article's Creative Commons licence, unless indicated otherwise in a credit line to the material. If material is not included in the article's Creative Commons licence and your intended use is not permitted by statutory regulation or exceeds the permitted use, you will need to obtain permission directly from the copyright holder. To view a copy of this licence, visit http://creativecommons.org/licenses/by/4.0/.

REFERENCES

1. International Energy Agency, iron and steel technology roadmap towards more sustainable steelmaking, 2020. https://iea.blob.core.windows.net/assets/eb0c8ec1-3665-4959-97d0-187ceca189a8/Iron_and_Steel_Technology_Roadmap.pdf. Accessed 6 August 2025.
2. E. Basson: World steel in figures, 2025. https://worldsteel.org/wp-content/uploads/World-Steel-in-Figures-2025-3.pdf. Accessed 2 July 2025.
3. A. Kumar: *Trans. Indian Inst. Metals*, 2024, vol. 77, pp. 4279–92. https://doi.org/10.1007/s12666-023-02978-2.
4. T. Ariyama: *ISIJ Int.*, 2025, vol. 65, no. 2, pp. 165–84. https://doi.org/10.2355/isijinternational.ISIJINT-2024-320.
5. Y. Chen and H. Zuo: *Ironmak. Steelmak.*, 2020, vol. 48, no. 6, pp. 749–68. https://doi.org/10.1080/03019233.2021.1909992.
6. V. Shatokha: *ISIJ Int.*, 2024, vol. 64, no. 14, pp. 1945–55. https://doi.org/10.2355/isijinternational.ISIJINT-2024-145.
7. Z. Li, Z. Qi, Z. Wang, L. Zhang, D. Liang, and Q. Dong: *Int. J. Hydrog. Energy.*, 2022, vol. 47, no. 73, pp. 31109–28. https://doi.org/10.1016/j.ijhydene.2022.07.036.
8. A. Babich, S. Yaroshevskii, A. Formoso, A. Cores, L. García, and V. Nozdrachev: *ISIJ Int.*, 1999, vol. 39, pp. 229–38. https://doi.org/10.2355/isijinternational.39.229.
9. K. Wang, J. Zhang, H. Zhou, J. Ni, Y. Hu, Y. Huang, J. Huang, S. Li, X. Ma, S. Wu, and M. Kou: *Appl. Therm. Eng.*, 2023, vol. 230, no. B, p. 120817. https://doi.org/10.1016/j.applthermaleng.2023.120817.
10. M. Asanuma, T. Ariyama, M. Sato, R. Murai, T. Nonanka, I. Okochi, H. Tsukiji, and K. Nemoto: *ISIJ Int.*, 2000, vol. 40, no. 3, pp. 244–51. https://doi.org/10.2355/isijinternational.40.244.
11. H. Nogami, Y. Kashiwaya, and D. Yamada: *ISIJ Int.*, 2012, vol. 52, no. 8, pp. 1523–27. https://doi.org/10.2355/isijinternational.52.1523.
12. C. Kamijo, Y. Matsukura, H. Yokoyama, K. Sunahara, K. Kakiuchi, H. Sakai, K. Nakano, Y. Ujisawa, and K. Nishioka: *ISIJ Int.*, 2022, vol. 62, no. 12, pp. 2433–41. https://doi.org/10.2355/isijinternational.ISIJINT-2022-099.
13. F. Mauret, J. Ji, P. Kinzel, H. Saxén, and M. Baniasadi: *ISIJ Int.*, 2025, vol. 65, no. 5, pp. 601–12. https://doi.org/10.2355/isijinternational.ISIJINT-2025-041.
14. F. Mauret, M. Baniasadi, H. Saxén, A. Feiterna, and S. Hojda: *Metall. Mater. Trans. B.*, 2023, vol. 54B, pp. 2137–58. https://doi.org/10.1007/s11663-023-02822-4.
15. A. Poos, N. Ponghis, N. de Woot, and A. Thirion: *Ironmaking Proceddings*, 1973, pp. 306–325.
16. J. Li, S. Kuang, R. Zou, and A. Yu: *Metall. Mater. Trans. B.*, 2023, vol. 54B, pp. 913–27. https://doi.org/10.1007/s11663-023-02735-2.
17. Z. Zhao, X. Yu, Y. Li, J. Zhu, and Y. Shen: *Fuel*, 2023, vol. 348, p. 128641. https://doi.org/10.1016/j.fuel.2023.128641.
18. P.R. Austin, H. Nogami, and J.-I. Yagi: *ISIJ Int.*, 1998, vol. 38, no. 3, pp. 239–45. https://doi.org/10.2355/isijinternational.38.239.
19. M. AbdulQuader, A. Shamsuddin, S. Dawal, and Y. Nukman: *Renew. Sustain. Energy Rev.*, 2016, vol. 55, pp. 537–49. https://doi.org/10.1016/j.rser.2015.10.101.
20. S. Angeli, S. Gossler, S. Lichtenberg, G. Kass, A. Agrawal, M. Valerius, P. Kinzel, and O. Deutschmann: *Angew. Int. Ed. Chem.*, 2021, vol. 60, pp. 11852–57. https://doi.org/10.1002/anie.202100577.
21. T. Miyashita, K. Sano, H. Nishio, S. Ohzeki, T. Nayuki, and L. Chaussy: *ISIJ Int.*, 1974, vol. 14, no. 3, pp. 176–84. https://doi.org/10.2355/isijinternational1966.14.176.
22. P. Blanck, G. Kass, K.-P. Kinzel, and O. Deutschmann: *Energy Adv.*, 2024, vol. 3, p. 123. https://doi.org/10.1039/D3YA00227F.
23. Y. Kawashiri, T. Nouchi, and Y. Kashihara: *JFE Techn. Rep.*, 2022, vol. 28, pp. 9–15.
24. J. Feinman: *Plasma Technology in Metallurgical Processing*, Iron and Steel Society of AIME, Warrendale, 1987.
25. M. Yakeya, A. Kasai, M. Sakamoto, T. Tagawa, and K. Miyata: *9th ECIC Proceedings*, 2024, pp. 1–5.
26. T. Norgate, N. Haque, M. Somerville, and S. Jahanshahi: *ISIJ Int.*, 2012, vol. 52, no. 8, pp. 1472–81. https://doi.org/10.2355/isijinternational.52.1472.

27. C. Wang, P. Mellin, J. Lövgren, L. Nilsson, W. Yang, H. Salman, A. Hultgren, and M. Larsson: *Energy Convers. Manag.*, 2015, vol. 102, pp. 217–26. https://doi.org/10.1016/j.enconman.2015.04.013.
28. D. Leeson, N. MacDowell, N. Shah, C. Petit, and P. Fennell: *Int. J. Greenh. Gas Control.*, 2017, vol. 61, pp. 71–84. https://doi.org/10.1016/j.ijggc.2017.03.020.
29. J. Perpiñán, B. Peña, M. Bailera, V. Eveloy, P. Kannan, A. Raj, P. Lisbona, and L.-M. Romeo: *Fuel*, 2023, vol. 336, p. 127074. https://doi.org/10.1016/j.fuel.2022.127074.
30. L. Frattini, V. Becattini, and M. Mazzotti: *Int. J. Greenh. Gas Control.*, 2024, vol. 136, p. 104172. https://doi.org/10.1016/j.ijggc.2024.104172.
31. International Energy Agency, Global Hydrogen Review 2023, 2023. https://iea.blob.core.windows.net/assets/ecdfc3bb-d212-4a4c-9ff7-6ce5b1e19cef/GlobalHydrogenReview2023.pdf. Accessed 28 August 2025.
32. International Energy Agency, Global Hydrogen Review 2024, 2024. https://iea.blob.core.windows.net/assets/89c1e382-dc59-46ca-aa47-9f7d41531ab5/GlobalHydrogenReview2024.pdf. Accessed 01 October 2025.
33. S. Nicholas, and S. Basirat: Iron ore quality a potential headwind to green steelmaking technology and mining options are available to hit net-zero steel targets, Institute for Energy Economics and Financial Analysis, 2022. https://ieefa.org/sites/default/files/2022-06/Iron%20Ore%20Quality%20a%20Potential%20Headwind%20to%20Green%20Steelmaking_June%202022.pdf. Accessed 01 October 2025.
34. G. Wimmer, B. Voraberger, B. Kradel, and A. Fleischanderl: *Tech. Rev.—Mitsubishi Heavy Ind.*, 2022, https://doi.org/10.1007/s11663-018-1332-6.
35. K. Yang, S. Choi, J. Chung, and J.-I. Yagi: *ISIJ Int.*, 2010, vol. 50, no. 7, pp. 972–80. https://doi.org/10.2355/isijinternational.50.972.
36. X. Yu and Y. Shen: *Metall. Mater. Trans. B.*, 2018, vol. 49B, pp. 2370–88.
37. Y. Hashimoto, Y. Sawa, Y. Kitamura, T. Nishino, and M. Kano: *ISIJ Int.*, 2018, vol. 58, no. 12, pp. 2210–18. https://doi.org/10.2355/isijinternational.ISIJINT-2018-177.
38. J.-P. Simoes, P. Tockert, L. Hausemer, C. Bodeving, P. Bermes, and V. Oliveira: BF process technology enhanced by charging control, process monitoring and mathematic models, in *Proceedings of the Ironmaking, Iron Ore and Agglomeration Seminars*, 2013.
39. C. Kamijo, H. Yokoyama, K. Kakiuchi, H. Sakai, Y. Matsukura, K. Sunahara, and K. Nakano: *Nippon Steel Techn. Rep.*, 2022, vol. 127, pp. 21–28.
40. K. Nakano, H. Sakai, Y. Ujisawa, K. Kakiuchi, K. Nishioka, K. Sunahara, Y. Matsukura, and H. Yokoyama: *ISIJ Int.*, 2022, vol. 62, no. 12, pp. 2424–32. https://doi.org/10.2355/isijinternational.ISIJINT-2022-117.
41. J. Li, S. Kuang, L. Jiao, L. Liu, R. Zou, and A. Yu: *Fuel*, 2022, vol. 323, p. 124368. https://doi.org/10.1016/j.fuel.2022.124368.
42. Y.-Z. Pan, H.-B. Zuo, B.-X. Wang, J.-S. Wang, G. Wang, Y.-L. Liu, and Q.-G. Xue: *Ironmak. Steelmak.*, 2018, vol. 47, no. 2, pp. 322–27. https://doi.org/10.1080/03019233.2018.1493762.
43. EU Carbon Permits (Trading Economics, 2025). https://tradingeconomics.com/commodity/carbon. Accessed 01 October 2025.

Publisher's Note Springer Nature remains neutral with regard to jurisdictional claims in published maps and institutional affiliations.